Probing chaos by magic monotones

Kanato Goto,[1,*] Tomoki Nosaka,[1,2,†] and Masahiro Nozaki[1,2,‡]

[1]*RIKEN Interdisciplinary Theoretical and Mathematical Sciences (iTHEMS), Wako, Saitama 351-0198, Japan*

[2]*Kavli Institute for Theoretical Sciences and CAS Center for Excellence in Topological Quantum Computation, University of Chinese Academy of Sciences, Beijing 100190, China*

(Received 12 July 2022; accepted 20 October 2022; published 19 December 2022)

There is a property of a quantum state called "magic." As shown by the Gottesman-Knill theorem, so-called stabilizer states, which are composed of only Clifford gates, can be efficiently computed on a classical computer, and thus quantum computation gives no advantage. Nonstabilizer states are called magic states, which are necessary to achieve the universal quantum computation. Magic (monotone) is the measure of the amount of nonstabilizer resource, and it measures how difficult it is for a classical computer to simulate the state. We study magic of states in the integrable and chaotic regimes of the higher-spin generalization of the Ising model through two quantities: "mana" and "robustness of magic" (RoM). We find that in the chaotic regime, mana increases monotonically in time in the early-time region, and at late times these quantities oscillate around some nonzero value that increases linearly with respect to the system size. Our result also suggests that under chaotic dynamics, any state evolves to a state whose mana almost saturates the optimal upper bound; i.e., the state becomes "maximally magical." We find that RoM also shows similar behaviors. On the other hand, in the integrable regime, mana and RoM behave periodically in time in contrast to the chaotic case. In addition to mana and RoM, for the early-time behavior of magic, we study the stabilizer Rényi entropy, which can be numerically computed for larger systems than mana and RoM. In the anti-de Sitter/conformal field theory correspondence, classical spacetime emerges from the chaotic nature of the dual quantum system. Our results suggest that magic of quantum states is strongly involved in the emergence of spacetime geometry.

DOI: 10.1103/PhysRevD.106.126009

I. INTRODUCTION

The question of how spacetime emerges from a more fundamental, microscopic concept of quantum gravity is one of the most intriguing questions in modern physics. In the context of holography, or the anti-de Sitter/conformal field theory correspondence (AdS/CFT correspondence) [1–3], the properties of the classical spacetime emerge from the quantum nature of the dual CFTs. The connection between the quantum nature of the CFT and geometry of the dual spacetime has been examined by quantum information-theoretic notions such as "quantum entanglement" [4] and "computational complexity" [5]. In this paper, we add a new quantum information-theoretic notion called "magic" to this list, which can capture a classical feature of gravity, as shown in the latter part of this paper.[1]

Quantum entanglement captures one aspect of the quantumness of a state, i.e., how much quantum correlation the state has. It is known that a CFT state with high energy density holographically corresponds to a black hole spacetime. Such a high energy density state, even if it is initially a simple state, quickly evolves into highly entangled, very complex states. In the dual geometry, this property of the state is captured by the growing black hole interior [7]. This property of the classical spacetime can be measured by the holographic dual to entanglement entropy proposed in [4] in most cases.

However, quantum entanglement alone does not fully account for the rich structure of a quantum state, nor does it fully characterize the properties of the dual classical spacetime. In one case, while the quantum entanglement reaches its equilibrium value relatively quickly, the black hole interior continues to expand afterward, and hence the

*kanato.goto@riken.jp
†nosaka@yukawa.kyoto-u.ac.jp
‡masahiro.nozaki@riken.jp

[1]Reference [6] is a pioneering work on magic in a quantum system at the critical point. This work studied magic in the $\mathbb{Z}_3$ Potts model and a tensor network model of AdS/CFT.

quantum entanglement fails to capture the property of the classical spacetime [5,7].

It was proposed in [5] that this continued growth in the black hole interior reflects the growing "computational complexity" of the quantum state [8–11], which entanglement entropy cannot capture. For simplicity, let us consider a discrete system that consists of N qubits. A local unitary operator that interacts with only a few neighboring sites is called a gate. A computational complexity is defined as the minimum number of gates required to build a target quantum state from a fixed reference state. In the chaotic system, one can expect that the complexity of a state grows linearly in time since a gate per second acting on a state will give us a new state that is different from the original state.

The holographic counterpart of the computational complexity for the CFT state dual to a AdS black hole was proposed in [12,13]. It is given by the gravitational action evaluated in the black hole interior (or more precisely, the so-called Wheeler–de Witt patch in the black hole spacetime).[2] Since the size of the black hole interior measured by this action grows linearly in time, it correctly reproduces the typical behavior of complexity in chaotic systems.

Magic, which we study in this paper, measures the complexity of quantum states that cannot be diagnosed by quantum entanglement or computational complexity. To introduce magic, let us classify all operations used in quantum computations into the stabilizer operations and the others. Stabilizer operations consist of the unitary type called Clifford operations, the injection of states in the Pauli basis, and the projection measurement in Pauli operators, all of which can be efficiently simulated on a classical computer, although some of them can generate quantum entanglement [16,17].[3] The states that they generate are called stabilizer states. This suggests that entanglement entropy[4] (which measures only the amount of quantum entanglement) or computational complexity (which counts all gates equally) cannot distinguish whether a quantum state is indeed complex in the sense that it is difficult to perform classical calculations at high speed.[5] Such complexity is produced by the non-Clifford gates. We will explain the Pauli operators, Clifford operations, and stabilizer states in detail in Secs. II A and II D.

To achieve the universal quantum computation we also need the non-Clifford unitary gates, which can be realized by the injection of nonstabilizer states (called magic states) combined with the stabilizer operations [23]. Magic is the measure of the amount of a nonstabilizer resource, and intuitively, it is a property of a state that describes how difficult it is to simulate the state on a classical computer. Roughly speaking, the difficulty to simulate a state $|\psi\rangle$ is measured by how many copies of reference nonstabilizer states one needs to prepare as an initial state to obtain $|\psi\rangle$ from the initial state through the stabilizer operations.[6]

In this paper, we evaluate magic through the quantities called mana and robustness of magic.[7] In particular, we are interested in the relation between magic and the chaotic property of a system. The definitions of mana and RoM are explained in Secs. II B and II C, respectively. To this end, we study mana and RoM in the higher-spin generalization of the Ising model, which has the chaotic and integrable (nonchaotic) regimes depending on the values of the parameters.

This model may not have a classical gravity dual since it only has small degrees of freedom, and the dual gravity theory would become strongly coupled. However, for specific choices of the values of the parameters, as we explained, the dynamics of this system becomes chaotic and captures one of the characteristic properties of classical gravity.

In this paper, we find that in the chaotic parameter regime, the states evolve to almost maximally magical states, suggesting that the chaotic property is closely related to magic of a quantum state [29,30]. From this result, we expect that magic is an important building block of classical spacetime, with the same basis as quantum entanglement and computational complexity.

We study the time evolution of pure-state mana and RoM in the higher-spin generalization of the Ising model [31]. This model is integrable when the transverse magnetic field h_x is turned off. If the spin of each site is $J = 1/2$, this model is also integrable when the longitudinal magnetic field h_z vanishes while h_x is nonzero. When (h_x, h_z) are not close to these points, on the other hand, the model is chaotic. In the latter two cases, the chaotic property of the model is reflected well in the level statistics: When $J = 1/2$ and $h_z = 0$, the level statistics coincides with that of the set of independent random numbers, while when $J \geq 1$ and $h_z = 0$ or when both of h_x, h_z are nonzero [in particular, around $(h_x, h_z) = (-1.05, 0.5)$], the level statistics agrees with that of the random matrix theory with the Gaussian orthogonal ensemble (GOE). We study how the behavior of mana and RoM depends on the dynamics of the system.

[2]Recent studies [14,15] pointed out that there are many ambiguities in this definition of the holographic complexity, but their details are out of the scope of this paper.

[3]Here, efficient means that a quantum computer consisting of n-qubits can be computed in n polynomial time on a classical computer.

[4]However, a series of papers [18–21] suggest the relation between the fluctuation property of the entanglement spectrum of a state generated by a circuit and the non-Cliffordness of the circuit.

[5]For a related work, see also [22].

[6]The minimum number of stabilizer states required to expand a quantum state is called the stabilizer rank χ, which is also one of the indicators for quantifying magic [24,25]. With χ, we can estimate the time it would take to simulate a quantum state on a classical computer.

[7]There are also several other quantities measuring magic (see, for example, Refs. [26–28]).

The main results obtained in the analysis of the time evolution of mana and RoM in Sec. IV are as follows: We found that the time evolution of mana and RoM depends on the chaotic property of the dynamics. At early times, both mana and RoM increase monotonically, and at late times of the chaotic regime, mana and RoM oscillate between the maximum values and the nonzero minimum values. We find that these maxima and minima are almost the same regardless of the choice of the initial state.[8] On the other hand, in the integrable regime, both mana and RoM behave periodically and depend on the initial states. Hence, the typical minimum values of mana and RoM at sufficiently late times are larger in the chaotic regime than in the integrable regime. We also observe that in the chaotic regime, the late-time maximum value of mana almost saturates the optimal bound that would be determined by the number of sites and the dimension of one-site Hilbert space. As the number of sites increases, the typical minimum value of mana at late times approximately coincides with the maximum value. These results suggest that under the chaotic dynamics, any state evolves to a state which almost saturates the optimal bound of mana.

In Sec. IV we also study the time evolution of mana and RoM when the open boundary condition and the periodic boundary condition are imposed on the system, and we find that the late-time behavior of these quantities does not depend significantly on the boundary condition.

Holographic systems describing classical gravity have large degrees of freedom. It is difficult to make accurate predictions for such systems from those with small degrees of freedom that we analyze in this paper. However, once mana is properly defined in the holographic systems, we expect that it will encode some geometrical information in anti-de Sitter space, as entanglement entropy and computational complexity do.

With this in mind, in Sec. V, we comment on some possible behaviors of mana in the holographic systems, including the following three possibilities: (1) Mana grows fast at early times and gradually slows down, as observed in the chaotic regime of the higher-spin generalized Ising model; (2) mana grows linearly in time until it saturates the upper bound derived from Jensen's inequality in Sec. II B (and also its holographic version in Sec. V); (3) the exponential of mana, not mana itself, grows linearly in time until it saturates the upper bound. In this section, we consider the time evolution of mana for a quenched thermofield double state in a two-dimensional conformal field theory with gravity dual (so-called holographic CFT). It is known that this state describes a wormhole spacetime that continues to grow linearly with time via holography.

Under some assumptions, we estimate the saturation time of mana in cases 2 and 3.

In case 1, the time dependence of mana differs from the linear growth of the wormhole captured by computational complexity (as well as entanglement entropy at early times). This suggests that the gravitational counterpart of mana, even if it exists, is not a simple quantity to measure the size of the wormhole.

In case 2, we estimate that mana would reach the upper bound in a polynomial time of the system size. In this case, the time dependence of mana deviates from that of complexity at a relatively early time, suggesting that the state largely deviates from the ones that can be efficiently simulated on a classical computer after that time.

In case 3, mana would reach the upper bound in an exponential time of the system size. In this case, the time dependence of mana does not deviate from that of complexity. This suggests that the early-time nonstabilizerness of the density matrix increases in time and that it saturates at exponential time of the system size. This fact is supported by the numerical computation on mana and another magic monotone called stabilizer Rényi entropy [28].

So far, we have described the background of this study and the results obtained. In Sec. II, we explain the aspect of magic as the resource of quantum computation and the definition of two physical quantities, mana and RoM, that measure magic. In Sec. III, we describe the higher-spin generalized Ising model. In Sec. IV, we numerically study the time dependence of mana and RoM in the chaotic and integrable regimes of the higher-spin generalized Ising model. We comment on the observations and some possible interpretations obtained from the numerical plots. In Sec. V, we comment on several possibilities of the behavior of mana in the holographic systems. We estimate the time when mana saturates its upper bound under some assumptions. We also approximate the early-time behavior of mana numerically computed by the linear function of time, and estimate the saturation time. In Sec. VI, we discuss the results of this paper and some future directions.

Some technical details which are not directly related to the analysis in the main text are allocated to the appendixes. In Appendix A, we display the initial state dependence of the late-time values of mana and robustness of magic. In Appendix B, we consider the small time expansion of mana $M(\rho(t))$ with the aim (though not successful) of understanding the linear growth of mana at early time observed in Sec. V.

II. MAGIC IN QUANTUM COMPUTATION

In this paper, we study how chaotic properties emerge from the quantum nature of a state through the notion of magic, which measures how difficult it is for a classical computer to simulate the state. The purpose of this section

[8]Here we have assumed that the initial state is not an energy eigenstate. In general, if there is a Hamiltonian (not necessarily of a spin chain), one of whose eigenstates has a small value of magic, the magic of that state remains low even at late times since the state is invariant under the time evolution of that Hamiltonian.

is to define two quantities that measure magic of states, mana and RoM, and to explain the resource aspect of magic. We study the time evolution of these quantities in a higher-spin generalized Ising model in the chaotic and nonchaotic parameter regimes in Sec. IV. In Sec. II A, we first introduce the Clifford operations, which are (parts of) the classical operations, and the stabilizer states generated by the Clifford operations. Then, in Secs. II B and II C, we introduce mana and RoM. Finally, in Sec. II D, we mention some aspects of magic in the framework of resource theory.

A. Clifford group and stabilizer states

To introduce the notion of magic, which measures how difficult it is for a classical computer to simulate the state, we first explain the Clifford group and the stabilizer states, the states which can be efficiently computed on a classical computer.

Let us consider a quantum system with d orthonormal states (we assume d to be a prime number) $|k\rangle$ $(k = 0, 1, \ldots, d-1)$ and a pair of operators z, x acting on this system,

$$z = \sum_{k=0}^{d-1} \omega^k |k\rangle\langle k| \ (\omega = e^{\frac{2\pi i}{d}}),$$
$$x = \sum_{k=0}^{d-1} |(k+1) \bmod d\rangle\langle k|. \tag{2.1}$$

Note that x, z satisfy the following properties:

$$x^d = z^d = 1, \qquad x^a z^b = \omega^{-ab} z^b x^a,$$
$$\mathrm{tr} z^a x^b = \begin{cases} d & (a,b) = (0,0) \bmod d \\ 0 & \text{otherwise,} \end{cases} \tag{2.2}$$

where a and b are integers. We also define the generalized Pauli operators $t_{aa'}$ as

$$t_{aa'} = \begin{cases} i^{aa'} z^a x^{a'} & d = 2 \\ \omega^{-\bar{2}aa'} z^a x^{a'} & d \geq 3, \end{cases} \tag{2.3}$$

where $\bar{2}$ is an integer such that $2 \times \bar{2} \equiv 1 \bmod d$. For general d, $t_{aa'}$ satisfies the following relations:

$$t_{aa'}^\dagger = t_{-a,-a'}, \qquad t_{aa'} t_{bb'} = \omega^{\bar{2}(ab'-ba')} t_{a+b,a'+b'} = \omega^{ab'-ba'} t_{bb'} t_{aa'}, \tag{2.4}$$

$$\mathrm{tr} t_{aa'} = \begin{cases} d & (a,a') = (0,0) \bmod d \\ 0 & \text{otherwise.} \end{cases} \tag{2.5}$$

In particular, $t_{aa'}$ are orthonormalized in the following sense:

$$\mathrm{tr}(t_{aa'} t_{bb'}^\dagger) = \begin{cases} d & (a,a') = (b,b') \bmod d \\ 0 & \text{otherwise.} \end{cases} \tag{2.6}$$

We consider a system that consists of L sites of this generalized qubit (or "qudit") whose Hilbert space is spanned by $\{|k_1\rangle \otimes |k_2\rangle \otimes \cdots \otimes |k_L\rangle\}$, and we consider the generalized Pauli operators (generalized Pauli strings) acting on these states labeled by $\vec{a} = ((a_1, a_1'), (a_2, a_2'), \ldots, (a_L, a_L'))$:

$$T_{\vec{a}} = t_{a_1 a_1'} \otimes t_{a_2 a_2'} \otimes \cdots \otimes t_{a_L a_L'}. \tag{2.7}$$

The Clifford group C_d is a discrete set of unitary matrices such that each element of C_d transforms the set of all Pauli strings $\{T_{\vec{a}}\}$ to itself up to some overall phases:

$$U \in C_d \Leftrightarrow U T_{\vec{a}} U^\dagger = e^{i\phi_U(\vec{a})} T_{\sigma(\vec{a})} \quad \text{for all } \vec{a}, \tag{2.8}$$

where $e^{i\phi_U(\vec{a})}$ are some phases and σ_U is a permutation on d^L choices of $\vec{a}$. The symbol ϕ is a real number. Explicitly, the Clifford group C_d for $d = 2$ is generated by the following elements, $R_a, P_a, \mathrm{SUM}_{a,b}$, which are, respectively, called the Hadamard gate, phase gate, and controlled-NOT gate[9] [32]:

(i) R_a, P_a $(a = 1, 2, \ldots, L)$:

$$R_a = 1 \otimes \cdots 1 \otimes R_a \otimes 1 \otimes \cdots 1,$$
$$P_a = 1 \otimes \cdots 1 \otimes P_a \otimes 1 \otimes \cdots 1, \tag{2.9}$$

with

$$R = \frac{1}{\sqrt{2}} \begin{pmatrix} 1 & 1 \\ 1 & -1 \end{pmatrix}, \qquad P = \begin{pmatrix} 1 & 0 \\ 0 & i \end{pmatrix}, \tag{2.10}$$

(ii) $\mathrm{CNOT}_{a,b}$ $(a, b = 1, 2, \ldots, L)$:

$$\mathrm{CNOT}_{a,b} : (\cdots \otimes \underset{a}{|k_a\rangle} \otimes \cdots \underset{b}{|k_b\rangle} \cdots) \to (\cdots \otimes \underset{a}{|k_a\rangle} \otimes \cdots \underset{b}{|(k_a + k_b) \bmod 2\rangle} \cdots), \tag{2.11}$$

where $|k\rangle$ is the eigenstate of z with eigenvalue $z = \omega^k$, as introduced above (2.1).

On the other hand, the Clifford group C_d for $d > 3$ is generated by the following elements, $R_a, P_a, S_a, \mathrm{SUM}_{a,b}$ [33]:

(i) R_a, P_a, S_a $(a = 1, 2, \ldots, L)$:

$$R_a = 1 \otimes \cdots 1 \otimes \underset{a}{R} \otimes 1 \otimes \cdots 1,$$
$$P_a = 1 \otimes \cdots 1 \otimes \underset{a}{P} \otimes 1 \otimes \cdots 1,$$
$$S_a = 1 \otimes \cdots 1 \otimes \underset{a}{S} \otimes 1 \otimes \cdots 1 \tag{2.12}$$

[9]Here, we follow the notation of [32].

with

$$R = \frac{1}{\sqrt{d}}(\omega^{(k-1)(\ell-1)})_{0\le k,\ell\le d-1} = \frac{1}{\sqrt{d}}\begin{pmatrix} 1 & 1 & 1 & \cdots & 1 \\ 1 & \omega & \omega^2 & \cdots & \omega^{d-1} \\ 1 & \omega^2 & \omega^4 & \cdots & \omega^{2(d-1)} \\ & & \vdots & & \end{pmatrix},$$

$$P = (\omega^{\frac{k(k-1)}{2}}\delta_{k\ell})_{0\le k,\ell\le d-1} = \begin{pmatrix} 1 & 0 & \cdots & & & 0 \\ 0 & \omega & 0 & \cdots & & 0 \\ 0 & 0 & \omega^3 & 0 & \cdots & 0 \\ & & & \ddots & & \\ 0 & \cdots & & 0 & \omega^{\frac{(d-2)(d-3)}{2}} & 0 \\ 0 & \cdots & & & 0 & \omega^{\frac{(d-1)(d-2)}{2}} \end{pmatrix},$$

$$S = (\delta_{k-a\ell,d\ (\mathrm{mod}\ d)})_{1\le k,\ell\le d-1}, \tag{2.13}$$

where a on the right-hand side of S is an integer such that $\{a, a^2, a^3, \cdots\}(\mathrm{mod}\ d) \supset (\mathbb{Z}_d\backslash\{0\})$. One can choose any a satisfying this condition. For example, for $d = 3$, the choice $a = 2$ works since all the elements of $\mathbb{Z}_d\backslash\{0\} = \{1, 2\}$ can be realized as $a^2 = 4 \equiv 1$, $a = 2$.

(ii) SUM gate $\mathrm{SUM}_{a,b}$ $(a, b = 1, 2, \ldots, L)$:

$$\mathrm{SUM}_{a,b}\colon (\cdots \otimes \underset{a}{|k_a\rangle} \otimes \cdots \underset{b}{|k_b\rangle}\cdots) \to (\cdots \otimes \underset{a}{|k_a\rangle} \otimes \cdots \underset{b}{|(k_a + k_b)\ \mathrm{mod}\ d\rangle}\cdots). \tag{2.14}$$

Choose one of the eigenstates of any single generalized Pauli operator as a base state. Here, let us choose $|\vec{0}\rangle = |0\rangle \otimes |0\rangle \otimes \cdots \otimes |0\rangle$ as the base state. The set of all stabilizer states $\{|S\rangle\}$ is defined as the states generated by the elements of the Clifford group C_d acting on the base state:

$$\{|S\rangle\} = \{U|\vec{0}\rangle | U \in C_d\}. \tag{2.15}$$

For general d and L, the number of all stabilizer states is given as [34]

$$|\{|S\rangle\}| = d^L \prod_{n=1}^{L}(d^n + 1). \tag{2.16}$$

We also define the convex hull of the stabilizer pure states $\{|s\rangle\langle s|\}_{|s\rangle\in\{|S\rangle\}}$, which we call STAB:

$$\mathrm{STAB} = \left\{ \sum_i c_i |s_i\rangle\langle s_i| \,\middle|\, |s_i\rangle \in \{|S\rangle\}, c_i \ge 0, \sum_i c_i = 1 \right\}. \tag{2.17}$$

B. Mana

In this section, we introduce one of the measures for magic of a quantum state called mana. Since STAB is a convex hull spanned by the stabilizer pure states, it would be natural to expect that for a given state expanded in the basis of stabilizer states, the negative coefficients in the expansion can be used to quantify the discrepancy of the state from STAB. Indeed, both mana and robustness of magic are related to the negativity of the state in this sense.

To define mana, we first define the phase space point operator $A_{\vec{a}}$ by using the generalized Pauli strings (2.7) as

$$A_{\vec{a}} = d^{-L} T_{\vec{a}} \sum_{\vec{b}} T_{\vec{b}} T_{\vec{a}}^\dagger, \tag{2.18}$$

which satisfies[10]

$$A_{\vec{a}}^\dagger = A_{\vec{a}}, \qquad \mathrm{Tr} A_{\vec{a}} A_{\vec{b}} = \begin{cases} d^L & \vec{a} = \vec{b}\ \mathrm{mod}\ d \\ 0 & \text{otherwise.} \end{cases} \tag{2.20}$$

With these phase space point operators $A_{\vec{a}}$, we define discrete Wigner functions $W_\rho(\vec{a})$ of a given density state ρ as

$$W_\rho(\vec{a}) = \frac{1}{d^L}\mathrm{Tr}\rho A_{\vec{a}}. \tag{2.21}$$

Since a set of the phase space point operators $\{A_{\vec{a}}\}$ forms a complete orthonormal basis of $d^L \times d^L$ Hermitian matrices, this implies $\rho = \sum_{\vec{a}} W_\rho(\vec{a}) A_{\vec{a}}$. If we impose the normalization condition $\mathrm{tr}\rho = 1$, $\{W_\rho(\vec{a})\}$ satisfies $\sum_{\vec{a}} W_\rho(\vec{a}) = 1$. Then, we define mana $M(\rho)$ of a state ρ as the negativity of $\{W_\rho(\vec{a})\}$:

$$M(\rho) = \log \sum_{\vec{a}} |W_\rho(\vec{a})| = \log\left[1 + 2 \sum_{\substack{\vec{a} \\ (\mathrm{s.t.} W_\rho(\vec{a})<0)}} |W_\rho(\vec{a})|\right]. \tag{2.22}$$

[10]Note that by using (2.4), we can also write $A_{\vec{a}}$ as

$$A_{\vec{a}} = d^{-L} \bigotimes_{i=1}^{L} \left(\sum_{b,b'} \omega^{a_i b' - a_i' b} t_{bb'} \right). \tag{2.19}$$

This expression is useful for explaining (2.20).

For ρ being a pure state, it is known that $M(\rho) = 0$ if and only if ρ is a stabilizer pure state (discrete Hudson's theorem) [34]. Since STAB is the convex hull of the stabilizer pure states, this also implies that $M(\rho) = 0$ for any $\rho \in \mathrm{STAB}$. However, when ρ is a mixed state, $M(\rho) = 0$ does not necessarily imply $\rho \in \mathrm{STAB}$. In this sense, mana is not a faithful quantification of the nonstabilizerness of the states. Also, mana is defined only when the number of states d on a single site is odd. Nevertheless, mana is a useful measure to quantify magic of the state since the definition of mana does not involve any optimization over the large degrees of freedom, unlike robustness of magic (2.28) or the relative entropy of magic [35] (which we do not consider in this paper).

Note that mana $M(\rho)$ obeys the following inequality:

$$M(\rho) \le \frac{1}{2}(L \log d - S_2), \tag{2.23}$$

where S_2 is the Rényi entropy $S_2 = -\log \mathrm{tr}\rho^2$ which can also be written in $W_\rho(\vec{a})$ as

$$e^{-S_2} = d^L \sum_{\vec{a}} W(\vec{a})^2. \tag{2.24}$$

The inequality (2.23) can be shown by using the concavity of the function $f(x) = \sqrt{x}$ (Jensen's inequality). For more details of the derivation of the inequality, see [36].

Let us add some comments on the upper bound for the case where ρ is a pure state, $\rho = |\psi\rangle\langle\psi|$, which is of our main interest in the subsequent sections. In this case, Jensen's inequality reduces to

$$M(|\psi\rangle\langle\psi|) \le \frac{L}{2} \log d. \tag{2.25}$$

Note that the inequality (2.25) [also (2.23)] does not mean that there actually exists either a state that saturates the bound or an infinite series of states whose mana converges to the saturation of the bound. That is, the right-hand side of (2.25) may not be the optimal upper bound, which we call $M_0(d, L)$, on mana of the pure states in the qudit system with L sites. Indeed for $d = 3$ and $L = 1$, $M_0(d, L)$ is known to be [35][11]

$$M_0(3, 1) = \log\left(\frac{5}{3}\right), \tag{2.26}$$

which is smaller than $(1/2)\log 3$. To our knowledge, the optimal bound for $L \ge 2$ is still not known. Nevertheless, for $d = 3$, since there exists a state $|\psi\rangle = |\mathbb{S}\rangle^{\otimes L}$ where $|\mathbb{S}\rangle = |\mathbb{S}\rangle = (|1\rangle - |2\rangle)/\sqrt{2}$ is the state in the single qudit system with $M(|\mathbb{S}\rangle\langle\mathbb{S}|) = M_0(3, 1)$ (see [35]), whose mana is $M(|\psi\rangle\langle\psi|) = LM(|\mathbb{S}\rangle\langle\mathbb{S}|) = LM_0(3, 1)$, the optimal upper bound $M_0(3, L)$ must not be less than $LM_0(3, 1)$. Together with (2.25), we conclude that $M_0(3, L)$ is in the following window:

$$L \log\left(\frac{5}{3}\right) \le M_0(3, L) \le \frac{L}{2} \log 3. \tag{2.27}$$

In Sec. IV A, we will use this fact to interpret the numerical results in the chaotic regime of the higher-spin generalized Ising model.

C. Robustness of magic

We have defined mana, one of the measures for magic of a quantum state. Here, we introduce another measure called robustness of magic. Robustness of magic, $\mathrm{RoM}(\rho)$, of a given state ρ is defined as [38–41]

$$\mathrm{RoM}(\rho) = \inf\left\{ \sum_{\{|S\rangle\}(V_{|S\rangle}<0)} |V_{|S\rangle}| \,\middle|\, V_{|S\rangle} \in \mathbb{R}, \sum_{\{|S\rangle\}} B_{\vec{a},|S\rangle} V_{|S\rangle} = F_{\vec{a}}(\rho) \right\}, \tag{2.28}$$

where

$$B_{\vec{a},|S\rangle} = \mathrm{Tr}(T_{\vec{a}}|S\rangle\langle S|), \qquad F_{\vec{a}} = \mathrm{Tr}(T_{\vec{a}}\rho), \tag{2.29}$$

with the generalized Pauli strings $T_{\vec{a}}$ (2.7) and the stabilizer pure states $|S\rangle$ (2.15). Note that since $\{T_{\vec{a}}\}$ is a complete set of $d^L \times d^L$ matrices, the constraint $\sum_{\vec{b}} B_{\vec{a},|S\rangle} V_{|S\rangle} = F_{\vec{a}}(\rho)$ is equivalent to the following:

$$\rho = \sum_{\{|S\rangle\}} V_{|S\rangle} |S\rangle\langle S|. \tag{2.30}$$

That is, $\mathrm{RoM}(\rho)$ (2.28) directly measures the amount of the negative coefficients when ρ is expanded in $\{|s\rangle\langle s|\}_{|s\rangle \in \{|S\rangle\}}$ in the most optimal way.

D. Stabilizer formalism and magic monotone

We would also like to briefly comment on the stabilizer formalism and the resource theory of magic, which allows us to formulate the "nonstabilizerness" systematically.

Let us start with a brief explanation of the resource theory. The resource theory is an idea to classify the quantum states by using the following three notions: (i) a set of operations $\mathcal{C}$, which, in general, are non-invertible; (ii) free states $\mathcal{S}$, which can be created from any single state in $\mathcal{S}$ by full $\mathcal{C}$ acting on it; (iii) monotone, which is some quantity defined for any state so that it does not increase under $\mathcal{C}$ and that it vanishes for the elements in $\mathcal{S}$. The states that cannot be generated by $\mathcal{C}$ acting on any

[11]The optimal upper bound is also known for $d = 5$ and $L = 1$ as $M_0(5, 1) = \mathrm{Arcsinh}(3 + \sqrt{5}) - \log 5$ [37], which is smaller than $(1/2)\log 5$, the right-hand side of (2.25). However, we will not use this result in this paper.

free states are called resource states. A monotone is positive if (provided that the monotone is faithful) and only if the state in question is a resource state. From the definition of the monotones, it also follows that it is impossible to obtain a resource state by $\mathcal{C}$ acting on another resource state with a smaller monotone. In this sense, a monotone of a state ρ quantifies the diversity of the states that can be generated from ρ by using $\mathcal{C}$.

As a concrete example, let us explain the entanglement and the related notions, which will be more familiar to the reader in the language of the resource theory [42–45]. In the resource theory of entanglement, the role of $\mathcal{C}$ is played by the set of operations which consists of local operations and classical communication (LOCC) as operations to solve quantum entanglement of states. The free state $\mathcal{S}$ corresponds to the set of separable density matrices. Conversely, the resource states are the entangled states. A physical quantity with the properties of the monotone in the resource theory of entanglement is called an entanglement monotone [46,47]. The entanglement entropy is a typical example of the entanglement monotones for the pure states.

In the context of magic, the set of operations $\mathcal{C}$ corresponds to the stabilizer protocols, and the free state $\mathcal{S}$ corresponds to STAB (2.17). The stabilizer protocol is the set of operations that consists of the Clifford group and some additional operations (composition of any stabilizer state; projection measurement on a single site into any of the computational basis $|k\rangle$; a partial trace of a single site) [35]. The image of the stabilizer protocol acting on a set of states is, in general, smaller than the initial set, while the image of STAB is itself. These properties suggest that we can consider the stabilizer protocol and STAB as the elements of the resource theory [35,44]. A monotone of a given resource state indicates how many states can be generated by the stabilizer operations on this state. It also quantifies how many copies of the given resource state $|\psi\rangle$ are required to generate a fixed target resource state $|\phi\rangle$ (with a large monotone) by $\mathcal{C}$. This is a kind of efficiency of the universal quantum computation realized by the stabilizer operations together with the resource state $|\psi\rangle$, called stabilizer formalism [35]. In [35], the monotone and the resource states of the stabilizer operations are called the magic monotone and the magic states. Mana and RoM are examples of the magic monotone.

III. HIGHER-SPIN GENERALIZED ISING MODEL

As an example of the qudit system with adjustable quantum chaoticity, we consider the higher-spin generalized Ising model with the open and periodic boundary conditions [31]:

$$H=\begin{cases}\frac{2}{\sqrt{3}}\sqrt{J(J+1)}\left[-\sum_{n=1}^{L-1}G_z^{(n)}G_z^{(n+1)}-\sum_{n=1}^{L}(h_xG_x^{(n)}+h_zG_z^{(n)})\right] & \text{(open)}\\ \frac{2}{\sqrt{3}}\sqrt{J(J+1)}\left[-\sum_{n=1}^{L-1}G_z^{(n)}G_z^{(n+1)}-G_z^{(L)}G_z^{(1)}-\sum_{n=1}^{L}(h_xG_x^{(n)}+h_zG_z^{(n)})\right] & \text{(periodic)},\end{cases} \tag{3.1}$$

where $G_i^{(n)}$ are given as

$$G_i^{(n)}=\sum_{n=1}^{L}\otimes 1\otimes\cdots\otimes 1\underset{n}{G_i}\otimes 1\otimes 1\otimes\cdots\otimes\underset{L}{1}, \tag{3.2}$$

with G_i being the $2J+1$ dimensional representation of $SU(2)$ generators. If we choose the eigenstates of G_z, $\{|j=J\rangle,|j=J-1\rangle,\ldots,|j=-J\rangle\}$, as the basis of the single-site Hilbert space, then G_i takes the following form:

$$G_z=\begin{pmatrix}J & & & \\ & J-1 & & \\ & & \ddots & \\ & & & -J\end{pmatrix},\qquad G_x=\frac{1}{\sqrt{2}}\begin{pmatrix}0 & a_0 & 0 & \cdots & & & 0\\ a_0 & 0 & a_1 & 0 & \cdots & & 0\\ 0 & a_1 & 0 & a_2 & 0 & \cdots & 0\\ & \ddots & \ddots & \ddots & \ddots & & \end{pmatrix},$$
$$a_i=\sqrt{\frac{(2J-i)(i+1)}{2}}. \tag{3.3}$$

A. Chaotic property

The model (3.1) is trivially integrable when $h_x = 0$, while when $h_x \neq 0$ the chaotic property of this model varies depending on the values of h_x, h_z (and also on J). There are several different ways to characterize the chaoticity of quantum many-body systems. Here, let us adopt, as a diagnosis of quantum chaos, the nearest-neighbor spacing distribution (NNSD) of the energy spectrum $\{E_n\}_{n=1}^{\dim\mathcal{H}}$ [48,49], which is the value distribution of $\{E_n - E_{n-1}\}$ normalized by the average value of $E_n - E_{n-1}$ over n. It has been observed that the NNSD of the energy spectrum obtained by quantizing a classical integrable system obeys the Poisson distribution [50], while the energy spectrum obtained by quantizing a chaotic system shows a similar NNSD to that of the random matrix theory (RMT) with the ensemble determined by the time-reversal property of the system [51]. This characterization has also been found to be consistent with other characterizations using level statistics such as the onset of the RMT-like linear growth (ramp) of the spectral form factor and also with the characterization by the growth exponent of the connected part of the out-of-time-ordered correlator (quantum chaos exponent) [52], provided that all of these quantities, in comparison, are well defined [53,54].

To characterize the chaoticity of a system correctly by using NNSD, we have to follow the following prescriptions. First, if the system enjoys some discrete symmetry, we have to split the full spectrum into the irreducible sectors protected by the symmetry and define the level spacing distribution by using only the energy levels within each sector. Second, if the averaged eigenvalue density $\bar{\rho}(E)$ of each sector is not uniform, we have to perform a redefinition of eigenvalues $\tilde{E}_n = \int_{E_0}^{E_n} \bar{\rho}(E')dE'$, called unfolding [49], and define the level spacing as $\tilde{E}_n - \tilde{E}_{n-1}$ instead of $E_n - E_{n-1}$.

In the higher-spin generalized Ising model with open boundary condition (3.1), there is reflection symmetry $\mathcal{O}_P$ which exchanges the ith site with the $(L-i)$th site. Hence we have to split the energy spectrum into those of reflection-even eigenstates $\mathcal{O}_P|n\rangle = |n\rangle$ and those of reflection-odd eigenstates $\mathcal{O}_P|n\rangle = -|n\rangle$. This can be done, for example, by deforming the Hamiltonian as

$$H \to H + \Lambda\mathcal{O}_P \tag{3.4}$$

with Λ any number sufficiently larger than the original bandwidth, and collecting the energy levels around $E \sim \pm\Lambda$. For the periodic case, there is also the translation symmetry $\mathcal{O}_T$ which changes the ith site into the $((i+1) \bmod L)$th site. Since $\mathcal{O}_T$ does not commute with $\mathcal{O}_P$, a sector labeled by the eigenvalue of $\mathcal{O}_T$ does not always split into the $\mathcal{O}_P$-protected sectors. However, the $\mathcal{O}_T$-protected sector with $\mathcal{O}_T = 0$ transforms to itself under the reflection; hence this sector can be further decomposed into the $\mathcal{O}_P$-protected subsectors.[12] Lastly, when we take the parameter h_z to be zero, the Hamiltonian (both the open and periodic boundary conditions) is invariant under an additional transformation $\mathcal{O}_Y$: $(G_x^{(n)}, G_z^{(n)}) \to (G_x^{(n)}, -G_z^{(n)})$. The explicit expressions for the unitary matrix $\mathcal{O}_Y$ that realizes this symmetry transformation for $J = 1/2$, 1 are the following:

$$\mathcal{O}_Y(d=2) = \begin{pmatrix} 0 & -i \\ i & 0 \end{pmatrix}^{\otimes L}, \quad \mathcal{O}_Y(d=3) = \begin{pmatrix} 0 & 0 & 1 \\ 0 & 1 & 0 \\ 1 & 0 & 0 \end{pmatrix}^{\otimes L}. \tag{3.5}$$

This unitary matrix $\mathcal{O}_Y$ has eigenvalues ± 1 and commutes with the geometrical symmetry transformations $\mathcal{O}_P$ and $\mathcal{O}_T$.

By unfolding each sector, we obtain NNSD as displayed in Fig. 1. The results indicate that the higher-spin generalized Ising model is chaotic for $(J, h_x, h_z) = (1/2, -1.05, 0.5)$ and (1, 1, 0) [31,55], while the model is integrable for $(J, h_x, h_z) = (1/2, 1, 0)$ [55].

IV. TIME DEPENDENCE OF MANA AND ROM

The main aim of this paper is to elucidate how the chaotic property emerges from the quantum nature of a system through the notion of magic. For this purpose, we study the time evolution of mana and RoM introduced in the previous section for the chaotic and nonchaotic regimes of the higher-spin generalized Ising model.

In this paper, we identify the eigenstates of G_i, $|J\rangle, |j = J-1\rangle, \ldots, |j = -J\rangle$ with the computational basis $|k\rangle$ in (2.1) as $|k\rangle = |j = J+1-k\rangle$, and choose the stabilizer state $|S\rangle$ as the initial state (2.17) and evolve it under the Hamiltonian of the system: $e^{-iHt}|S\rangle$. For simplicity,[13] we choose $|x = \omega^{-1}\rangle \otimes |x = 1\rangle^{\otimes(L-2)} \otimes |x = \omega^{-1}\rangle$, where $|x = \omega^n\rangle$ is the eigenstate of x (2.1) with eigenvalue ω^n, as the initial stabilizer pure state $|S\rangle$. We abbreviate this state as $|x(d-1)x0\cdots x0x(d-1)\rangle\rangle$. In Secs. IV A and IV B, we display the results of the analysis. In Sec. IV C, we list the observations and their interpretations.

A. Mana

In Figs. 2 and 3, we display the results of mana for the generalized higher spin Ising model (3.1) with $J = 1$

[12]When L is even, this also applies to the $\mathcal{O}_T = -1$ sector.

[13]We choose a state that respects the reflection symmetry that exists for any choice of (J, h_x, h_z) to make the computation easier. At the same time, we avoid a state that reflects any of the enhanced global symmetry T, U that appears only when the system is periodic or when $h_x = 0$ so that the comparison of the results for the different chaotic models (open, open with $d = 3, h_x = 0$, closed, closed with $d = 3, h_x = 0$) would be more reasonable.

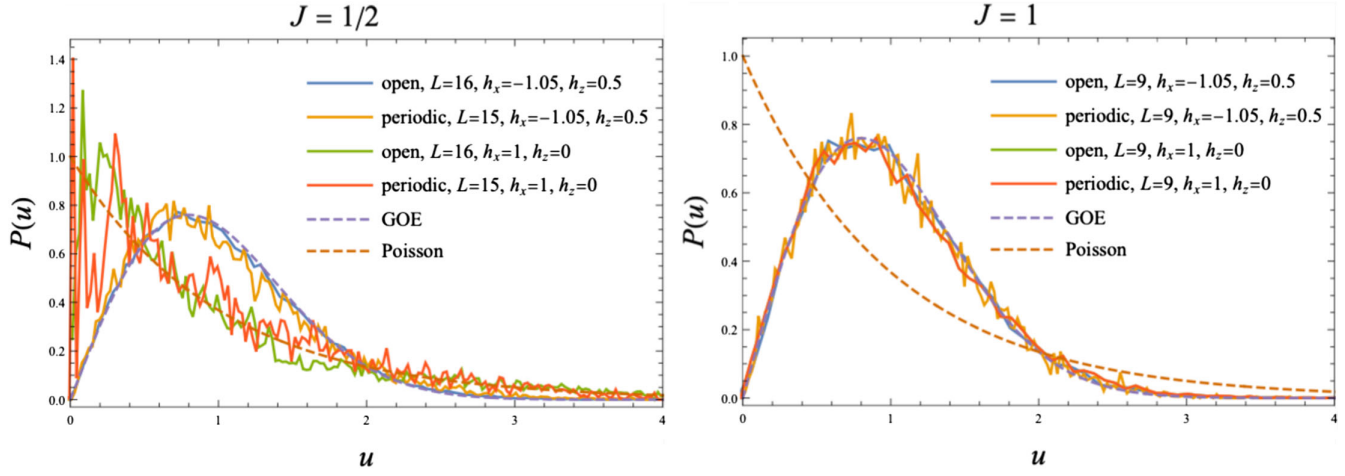

FIG. 1. NNSD of the higher-spin generalized Ising model with open and periodic boundary conditions (3.1). Here, u in the horizontal axis represents the values of $\tilde{E}_n - \tilde{E}_{n-1}$ normalized by the average over the subsector in concern. Each histogram is drawn by first computing the level spacings of the unfolded spectrum, normalizing in each sector separately, and then combining the results of all the subsectors. We chose the background magnetic fields as $h_x = -1.05, h_z = 0.5$ and $h_x = 1,\ h_z = 0$.

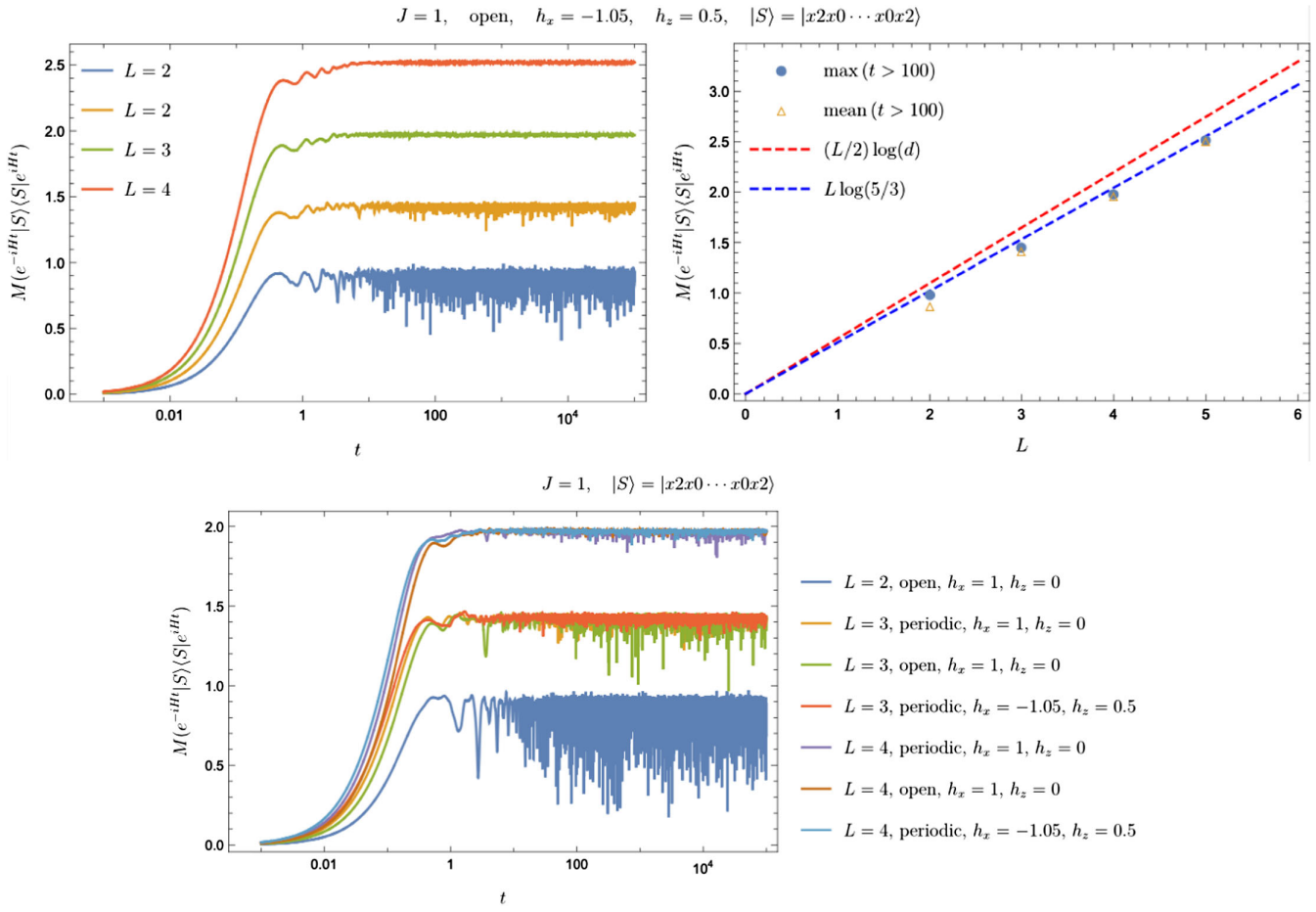

FIG. 2. Top left: time evolution of mana $M(e^{-iHt}|S\rangle\langle S|e^{iHt})$ with $J = 1$, $(h_x, h_z) = (-1.05, 0.5)$, and $|S\rangle = |x = \omega^{-1}\rangle \otimes |x = \omega^0\rangle^{\otimes(L-2)} \otimes |x = \omega^{-1}\rangle$. Top right: maximum value and the time average of $M(e^{-iHt}|S\rangle\langle S|e^{iHt})$ for $100 < t < 10^5$. Bottom: time evolution of mana for $h_x = -1.05, h_z = 0.5$ with a periodic boundary condition and for $h_x = 1, h_z = 0$ with open and periodic boundary conditions.

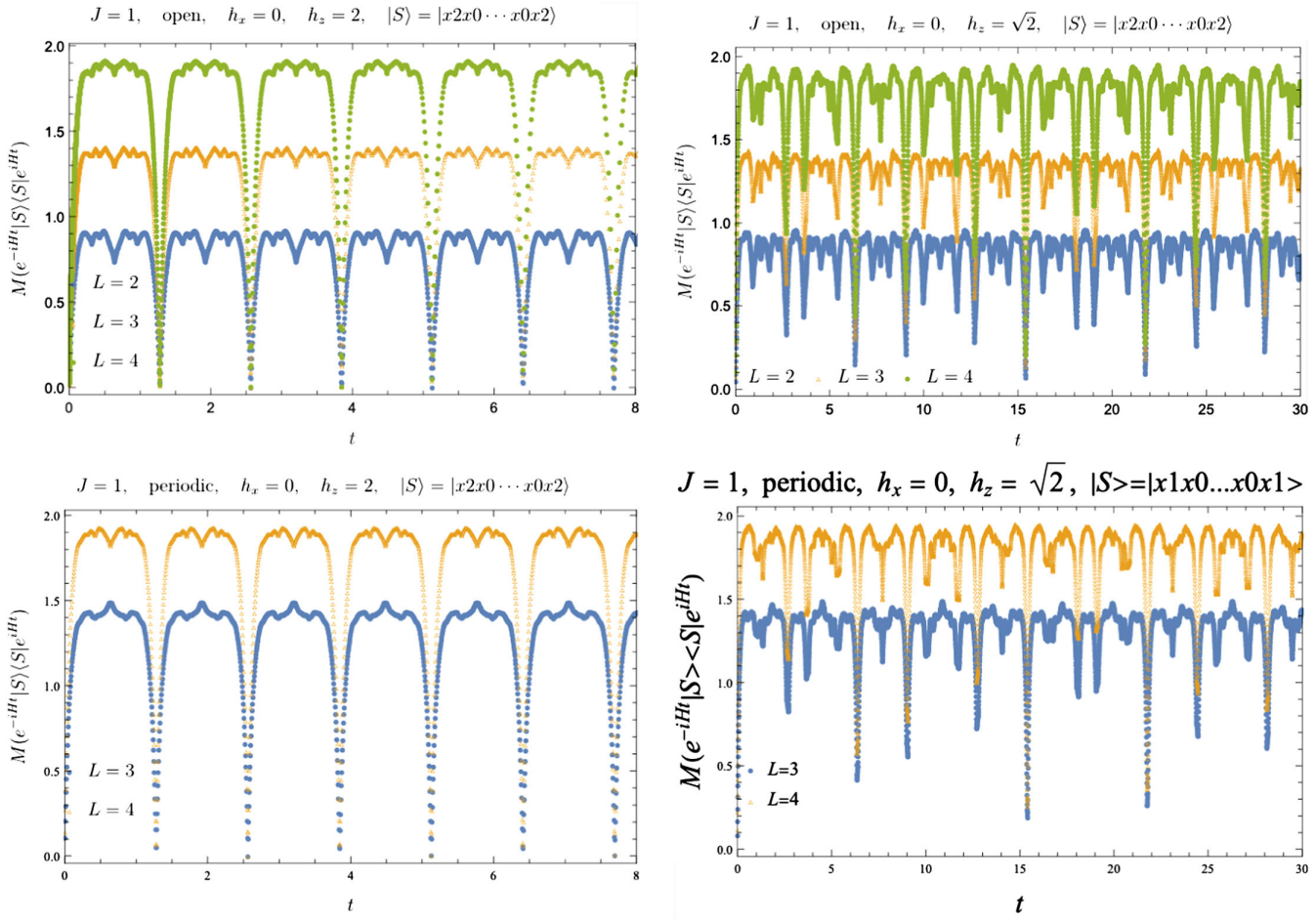

FIG. 3. Top left: time evolution of mana $M(e^{-iHt}|S\rangle\langle S|e^{iHt})$ with $J=1$, $(h_x,h_z)=(0,2)$, and $|S\rangle=|x=\omega^{-1}\rangle\otimes|x=\omega^{0}\rangle^{\otimes(L-2)}\otimes|x=\omega^{-1}\rangle$. Top right: same plot for $(h_x,h_z)=(0,\sqrt{2})$. Bottom left and bottom right: same plots for the periodic boundary condition.

(i.e., qudits with $d=3$) in the chaotic regime $(h_x,h_z)=(-1.05,0.5)$ and $(1,\ 0)$ and in the integrable regime $(h_x,h_z)=(0,2)$ and $(0,\sqrt{2})$.

In the chaotic regime $(h_x,h_z)=(-1.05,0.5),(1,0)$, we find that mana increases monotonically at early times and then oscillates erratically around some nonzero value. In particular, we observe that the minima of the oscillation are well separated from zero, the initial value of mana. We confirm that these behaviors are universal for a generic choice of $|S\rangle\in\{|S\rangle\}$ and that they do not depend on whether the boundary condition is open or periodic (see Appendix A). As the number of sites L increases, the maximum value of the oscillation also increases while the magnitude of the error becomes more and more suppressed. We also observe that the maximum value is very close to $L\log(5/3)$, the lower bound on the optimal upper bound $M_0(3,L)$ on mana of the pure states (2.27). Since the window for $M_0(3,L)$ (2.27) is narrow, this observation can also be rephrased such that the late-time maximum value almost saturates the actual optimal upper bound, although the precise value of $M_0(3,L)$ is still undetermined.

Here, purely based on the results of the numerical analysis, we propose, for finite d ($d=3$), that the late-time maximum of mana almost saturates the optimal upper bound. Note that for a chaotic system with $d\gg 1$ that enjoys Haar randomness, there is a different argument to justify the same statement as follows. Let us assume that mana becomes almost independent of the choice of the initial state at late times as we observed for $d=3$. Then, we would be able to evaluate the late-time mana of a single state as an average over the Haar random ensemble,

$$M(e^{-iHt}|\psi\rangle\langle\psi|e^{iHt})\approx\langle M(|\psi\rangle\langle\psi|)\rangle_{\mathrm{Haar}},\qquad(4.1)$$

where $\langle f(|\psi\rangle)\rangle_{\mathrm{Haar}}$ is defined as $\mathcal{N}\int_{\sum_i|\alpha_i|^2=1}\prod_i\frac{i|d\alpha_i|^2}{2}f(|\psi\rangle=\sum_i\alpha_i|i\rangle)$ with $\{|i\rangle\}$ an orthonormal basis and $\mathcal{N}$ the normalization constant. The right-hand side of (4.1) is calculated for $d\gg1$ [36] and is found to be $\langle M(|\psi\rangle\langle\psi|)\rangle_{\mathrm{Haar}}\approx(L/2)(\log d-\log\sqrt{\pi/2})$. Since this can be approximated in the large d limit by $(L/2)\log d$, i.e., the largest possible value for the optimal upper bound

$M_0(d, L)$ (2.25), we conclude that the late-time mana saturates $M_0(d, L)$.

In the integrable regime $(h_x, h_z) = (0, 2)$, we find that mana behaves periodically in time and returns to the initial value repeatedly. We also study an integrable regime with irrational coupling $(h_x, h_z) = (0, \sqrt{2})$ and find a similar behavior, although its time evolution is not completely periodic in this case. These results suggest that one can distinguish chaotic systems from integrable systems using mana.

B. Robustness of magic

In the previous section, we found that under chaotic dynamics, the state evolves from a stabilizer state, which can be efficiently simulated on a classical computer, to a state with an almost maximal value of mana. This fact is independent of the boundary conditions and suggests that under chaotic dynamics, except for exceptional states such as energy eigenstates, almost all states evolve to the most difficult state to simulate on a classical computer. To make sure that this correctly reflects the property of magic in the chaotic regime, rather than the particular property of mana, we study another magic measure, robustness of magic.

Let us consider the time evolution of RoM (2.28) of the state $\rho = e^{-iHt}|S\rangle\langle S|e^{iHt}$. The definition of the RoM involves the optimization over the space spanned by all of the stabilizer pure states. Since the number of stabilizer pure states increases quickly with respect to the number of sites L and the dimension of the single-site Hilbert space d as $|\{|S\rangle\}| = d^L \prod_{n=1}^{L}(d^n + 1)$ (2.16), the computation of RoM is difficult compared to mana for the same values of d and L. On the other hand, one advantage of studying RoM is that it can also be defined when d is in contrast to mana.

In Figs. 4–6, we display the results of the higher-spin generalized Ising model (3.1) for $(h_x, h_z) = (-1.05, 0.5)$, $(1, 0), (0, \sqrt{2})$ with $J = 1/2$, 1. We find that, at least for $(h_x, h_z) = (-1.05, 0.5)$ (chaotic regime) and $(h_x, h_z) = (0, \sqrt{2})$ (integrable regime), the time evolution of RoM exhibits similar behaviors as mana:

(i) For the chaotic case, RoM monotonically increases at early times, and it oscillates between the maximum value and the nonzero minimum value at late times. The maximal value of RoM becomes larger as L increases.

(ii) For the integrable case with $(h_x, h_z) = (0, \sqrt{2})$, RoM repeatedly comes close to zero in a short time.

(iii) RoM in the chaotic regime exhibits the same behavior for the open and the periodic boundary conditions. We also study the other choices of the initial stabilizer state and find similar results except for some exceptional cases. One case is that the initial state is an eigenstate of H, which does not evolve in time and always gives zero RoM. Another case is when the stabilizer pure state belongs to a sector protected by symmetry that consists only of two energy eigenstates. In this case, RoM behaves periodically, with the period given by the difference of the two energy eigenvalues (the same phenomenon can also be seen for mana).

For $(J, h_x, h_z) = (1, 1, 0)$, we find a qualitatively similar behavior of RoM in the case with $(J, h_x, h_z) = (1, -1.05, 0.5)$, which is consistent with the fact that the system is chaotic in both parameter regimes. On the other hand, for $(J, h_x, h_z) = (1/2, 1, 0)$ with $L = 3$ and the periodic boundary condition, we do not find a significant difference in the behavior of RoM from that for $(J, h_x, h_z) = (1/2, -1.05, 0.5)$, although the system is integrable in the former case. We expect that this is a finite L artifact because we also found that the behavior of

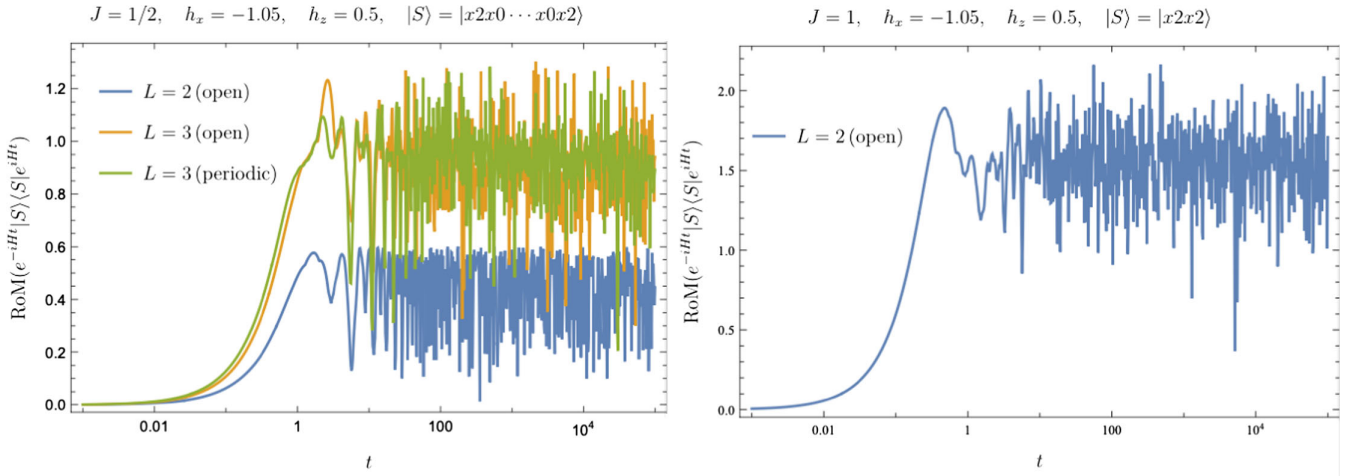

FIG. 4. In both the right and left panels, we show the time evolution of the RoM in the chaotic region. In the left panel, we take the parameters (J, h_x, h_z) to be $(1/2, -1.05, 0.5)$, while in the right panel, we take the parameters (J, h_x, h_z) to be $(1, -1.05, 0.5)$.

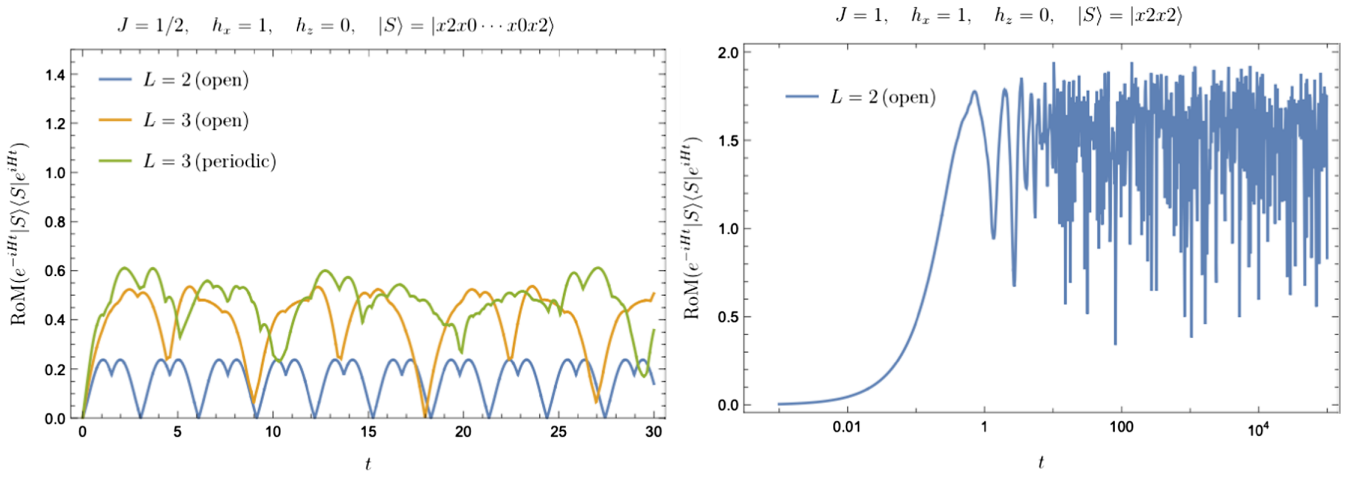

FIG. 5. Evolution of RoM in the higher-spin generalized Ising model with $(J, h_x, h_z) = (1/2, 1, 0)$ (left) and $(J, h_x, h_z) = (1, 1, 0)$ (right).

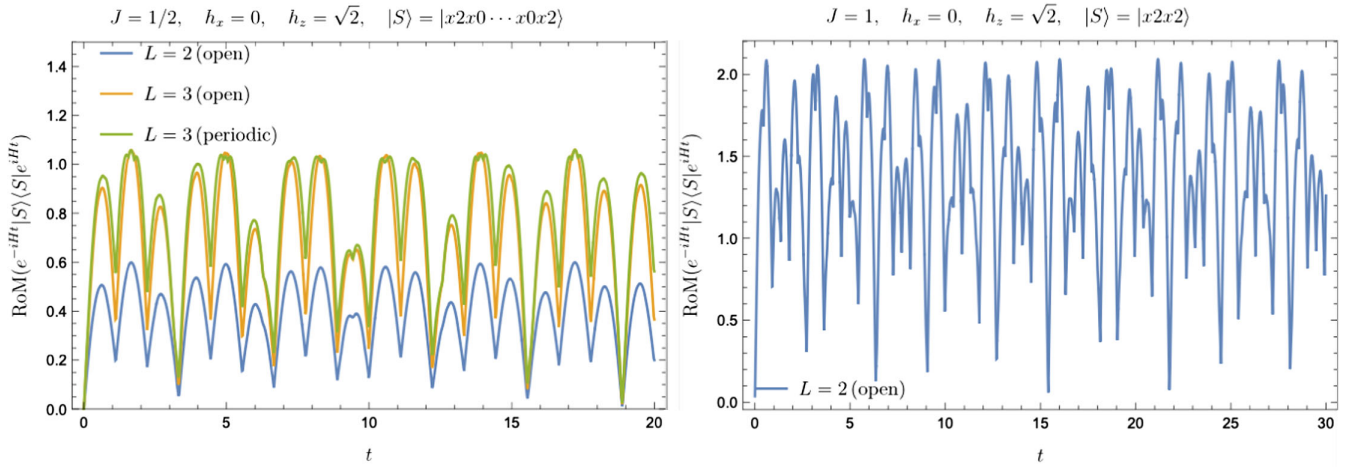

FIG. 6. Evolution of RoM in generalized higher-spin Ising model in the integrable regime, $(h_x, h_z) = (0, \sqrt{2})$. In both the right and left panels, we show the time evolution of the RoM in the integrable region. In the left panel, we take the parameters (J, h_x, h_z) to be $(1/2, 0, \sqrt{2})$, while in the right panel, we take the parameters (J, h_x, h_z) to be $(1, 0, \sqrt{2})$.

RoM for $(J, h_x, h_z) = (1/2, 1, 0)$ and $L = 3$ with the periodic boundary condition is different from that for $(J, h_x, h_z) = (1/2, 1, 0)$ and $L = 3$ with the open boundary condition, where RoM approaches zero as in the other integrable cases.

C. Observations and possible interpretations

We have seen the time dependence of mana and RoM in the chaotic and integrable regimes in the higher-spin generalized Ising model. Both quantities behave similarly, suggesting that they correctly capture how magic, the difficulty for a classical computer to simulate the state, evolves in time. However, we only computed them in the systems with such small degrees of freedom that there would be some subtleties in the interpretation of our results. Nevertheless, in this section, we try to describe what can be observed from the numerical plots shown above and some possible interpretations that can be read from them.

1. Observations

Here we briefly summarize some observations for the plots displayed in the previous section.

(i) Initial growth of mana

Here, we briefly discuss how the initial growth of the exponential of mana depends on the initial stabilizer pure states and the dynamics. Please see Appendix B for the details of the discussion. In the initial time region, $t \approx 0$, we observe that the initial growth of $e^{M(\rho(t))}$ is approximated by the linear function of t:

$$e^{M(\rho(t))} = 1 + \frac{t}{d^L}\sum_{\vec{a}}|\langle S|[H, A_{\vec{a}}]|S\rangle| + \mathcal{O}(t^2). \quad (4.2)$$

Thus, the coefficient of t in (4.2) is determined by the expectation value of $\frac{dA_{\vec{a}}(t)}{dt}|_{t=0}$, where $A_{\vec{a}}(t) = e^{-iHt}A_{\vec{a}}e^{iHt}$. Therefore, the initial growth of $e^{M(\rho(t))}$ depends on the initial stabilizer states and the Hamiltonian.

(ii) Chaos and magic

In the previous section, we numerically studied the time dependence of mana and RoM in the chaotic and the integrable regimes of the higher-spin generalized Ising model. We observed that the curves showing the time dependence of mana and RoM in the chaotic regime initially rise rapidly, then gradually slow down with time, and finally saturate to certain values. They behave similarly independent of the choices of the initial states and the boundary conditions except for some special cases. In particular, at late times, mana stops varying once it reaches the maximum that scales linearly in the number of sites with the coefficient almost coinciding with the optimal upper bound on mana for a single qudit system. In other words, at late times, mana almost saturates the optimal upper bound for the full L site qudit system.

On the other hand, mana and RoM in the integrable regime behave quite differently from the chaotic regime. They behave periodically with time and repeatedly transition between the states with large values and the ones with small values of mana and RoM and never converge to certain values. Their behavior strongly depends on the choices of the initial state and the boundary condition. The typical minimum values of mana and RoM at sufficiently late times are smaller than the chaotic regime.

2. Possible interpretations

(i) Maximally magical state as typical state

In a chaotic system, one can expect that almost all the states reach the typical states, which at least share the common features probed by some restricted set of physical observables. As we have seen in the above section, mana and RoM in the chaotic regime behave independently of the choices of the initial states and the boundary conditions. In this sense, at late times, almost all the states approach the typical states, which share the common feature from the perspective of magic. Moreover, at late times, mana almost saturates the optimal upper bound. This indicates the following statement: Typical states in the chaotic systems are almost maximally magical, at least, as probed by mana and RoM. This is one of the main findings of this paper. As described above, we also observe that in the integrable regime, mana and RoM behave periodically. This indicates that the states never settle down to the maximally magical state, in contrast to the chaotic regime, periodically transitioning between highly magical and less magical states.

(ii) Growth of the number of magic gates

In the plots described above, we can observe that at early times, mana and RoM grow rapidly in time and gradually slow down as time evolves. There might be some subtleties and finite L artifacts in our analyses, but if this is the case, it suggests that the number of magic gates required to construct a new time-evolved quantum state already almost saturates in the early stage of time evolution.

V. MAGIC IN HOLOGRAPHY

As we described in the Introduction, our original motivation was to understand the role of "quantumness" of the boundary nongravitational system in the emergence of classical spacetime geometry in the context of holography. The holographic duals to the entanglement entropy and computational complexity were proposed in the literature. They revealed intriguing connections between the quantum nature of the conformal field theories and the properties of spacetime geometry in anti–de Sitter space.

In the previous section, we numerically analyzed mana and RoM in the chaotic system with small degrees of freedom, which does not have a classical gravity dual. We expect that the behaviors of mana and RoM contain some artifacts due to the smallness in the degrees of freedom of the system. Therefore, it is difficult to accurately estimate their behavior in the holographic systems, i.e., chaotic systems with large degrees of freedom. Here, we only mention a few possibilities.[14] To make the discussion concrete, let us consider the holographic conformal field theories and focus on mana in the so-called (quenched) thermofield double state:

$$|\mathrm{TFD}(t)\rangle = \mathcal{N}e^{\frac{-(it+\beta)(H_1+H_2)}{2}}\sum_{E_a}|E_a\rangle_1 \otimes |E_a\rangle_2, \quad (5.1)$$

defined in the doubled Hilbert space $\mathcal{H} = \mathcal{H}_1 \otimes \mathcal{H}_2$. Here $|E_a\rangle_i$ is an eigenstate of Hamiltonian H_i with eigenvalue E_a in Hilbert space $\mathcal{H}_i$, β is the inverse temperature, and $\mathcal{N}$ is a normalization constant $\mathcal{N}^2 = (\sum_{E_a} e^{-\beta E_a})^{-1}$.

[14]Some of the readers might be concerned about whether mana and RoM can be defined in the holographic systems, i.e., continuum field theories without a clear notion of "qubits." In this section, we leave this issue as an interesting future direction and simply assume that mana and RoM are well defined in the holographic systems.

A. Upper bound on mana

Let us consider a chaotic discrete system with dimension d of local Hilbert space at each lattice site and the system size $2L$. If we assume[15] $d \gg 1$, we find, as commented in Sec. IV A, that mana of any state at late times would almost saturate Jensen's inequality: $M(t) \approx L \log d$. Notice that the right-hand side gives the thermal entropy S_{thermal} of the system. We expect that mana also satisfies this bound in the holographic systems. In particular, in a holographic two-dimensional conformal field theory, we have

$$M(t) \leq S_{\text{thermal}} = \frac{c\pi L}{3\beta} \tag{5.2}$$

with the central charge c of the conformal field theory, which would be saturated at late times.

B. Growth of mana

Growth of mana will give us important information about the geometrical structure in the anti–de Sitter space dual to the state (5.1). It is conjectured that the gravity dual to the state (5.1) is a wormhole connecting two outside regions, each of which is described by $\mathcal{H}_i$ of the dual quantum system. Therefore, if mana is properly defined in the holographic systems, its growth can capture the time dependence of some geometrical property of the wormhole.

We discuss several possibilities in the growth of mana in the holographic systems:

(1) Mana grows fast at early times and gradually slows down.

In the numerical analyses of the higher-spin generalized Ising model, we observe that mana (and RoM) grow rapidly at early times and gradually slow down as time evolves. There are ambiguities caused by the smallness in the degrees of freedom of the system, and the time dependence of mana in the holographic system is unclear. One of the most natural guesses is that it shows the same behavior observed in the higher-spin generalized Ising model: Mana first grows rapidly, gradually slows down, and asymptotically approaches its maximal value.

One of the most simple characteristics of the wormhole geometry dual to the thermofield double state (5.1) is its size, which grows linearly in time. This time dependence can be captured by entanglement entropy at the early stage of the time evolution and by computational complexity even at later stages.

If mana in the holographic systems indeed behaves as described above, this is in contrast to the time dependence of the size of the wormhole geometry dual to (5.1). This suggests that the gravitational counterpart of magic, if it exists, is not simply a measure of the size of the wormhole, in contrast to the case of entanglement entropy and computational complexity.

(2) Mana grows linearly in time until it saturates the bound.

While the growth of mana in the higher-spin generalized Ising model shows a nontrivial curve as explained above, in the early-time region it can be well approximated by a linear function as, in general, any smooth curves. Thus, one can imagine another scenario, where only the linearly growing regime in the system with small degrees of freedom is amplified, and the slowing-down regime is suppressed as we increase the degrees of freedom in the system. If this is the case, mana in the holographic system grows linearly as $M(t) \sim at + b$ and captures the linear growth in the size of the wormhole in time up to the time when it saturates the upper bound (5.2). In particular, one can estimate that the growth of mana stops at most polynomial times in S_{thermal}, assuming that a and b scale most in the polynomial of S_{thermal}, much earlier than the saturation time of the computational complexity. Let us remind ourselves that while the computational complexity counts all the gates equally, magic only counts the magic gates that cannot be efficiently simulated on a classical computer. Therefore, if mana follows the linear growth discussed above, it suggests that after a sufficiently long time, $t \gtrsim S_{\text{thermal}}^n$, the state largely deviates from the one that can be efficiently simulated on a classical computer. Here, n is an integer.

(3) Exponential of mana grows linearly in time until it saturates the bound.

The third possibility is that the exponential of mana, not mana itself, grows linearly in time as $e^{M(t)} \sim at + b$. This means the nonstabilizerness of the density matrix increases linearly in time because the mana is related to the logarithmic function of the density matrix as in (2.22). Assuming that a is, at most, given by the polynomial of S_{thermal} and $e^{S_{\text{thermal}}} \gg b$ in the limit $L \gg \beta$, we roughly estimate the saturation time as

$$t_{\text{saturation}} \sim e^{S_{\text{thermal}}}. \tag{5.3}$$

This is the same order as the saturation time of the computational complexity.

[15]This assumption is justified once we identify the qudit system with a holographic two-dimensional conformal field theory with central charge $c \gg 1$ at finite temperature β (normalized by the UV cutoff scale) through $d = e^{\pi c/(3\beta)}$ by identifying the thermal entropy of both systems as $L \log d = \frac{c\pi L}{3\beta}$ (L on the right-hand side is the one-dimensional volume divided by the UV cutoff, which corresponds to the number of lattice sites).

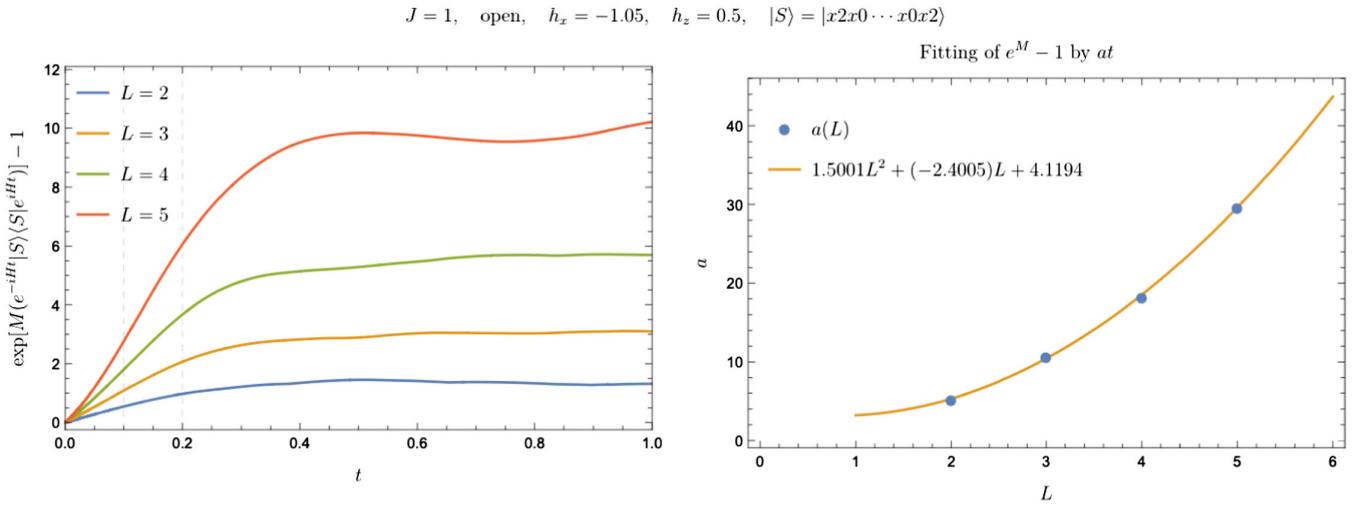

FIG. 7. Left: time evolution of $e^M - 1$. Right: rate of early-time linear growth of $e^M - 1$ obtained by fitting the data in $0.05 \le t \le 0.2$ for $L = 2$ and $0.1 \le t \le 0.2$ for $L = 3, 4, 5$.

1. Numerical supporting evidence

The assumption $e^{M(t)} \approx at + b$ is also supported by the numerical results for the spin system. Note that the initial states we have used in the numerical analysis are different from the thermofield double state (5.1). Nevertheless, here we assume that the behavior of mana is also qualitatively the same when the initial state is the thermofield double state. As displayed in Fig. 7, we observe that $e^{M(\rho=e^{-iHt}|S\rangle\langle S|e^{iHt})}$ grows linearly at early times, $e^M - 1 \approx at$ with a some constant. Here, the early-time growth of the exponential of mana is different from the initial growth in Sec. IV C. The early-time growth of the exponential of mana is in the time interval $0.05 \le t \le 0.2$ for $L = 2$ and $0.1 \le t \le 0.2$ for $L = 3, 4, 5$, while the initial time growth is at $t \approx 0$. Since at late times, mana oscillates erratically around some nonzero value, it would be natural to define the saturation time of mana for the higher-spin generalized Ising model as

$$t_{\text{saturation}} = \frac{e^{\max_{t>100}[M(\rho=e^{-iHt}|S\rangle\langle S|e^{iHt})]} - 1}{a}, \tag{5.4}$$

where $\max_{t>10}[M(\rho = e^{-iHt}|S\rangle\langle S|e^{iHt})]$ is the maximum value of mana at late times. In Figs. 7 and 8, we display the results of the fitting at early times and the L dependence of $t_{\text{saturation}}$ obtained. We find that as the number of sites L increases, both the early-time growth rate a and the saturation time $t_{\text{saturation}}$ increase. We further observe that as the number of sites L is increased, a scales as $a \sim L^2$.[16]

Combining this result with the observation that the late-time maximum $\max_{t>10}[M(\rho = e^{-iHt}|S\rangle\langle S|e^{iHt})]$ grows linearly in L (see Fig. 2), it follows that the saturation time scales exponentially in L. Note that there are several subtleties in our analysis in the higher-spin generalized Ising model. First, since our analysis is limited to the small system size $L \le 5$, it is not clear whether the L dependence of the growth coefficient $a(L)$ is really a polynomial in L. Also, even if the polynomial scaling is correct, the physical interpretation of the order of the polynomial and the coefficients of the polynomial are not clear. Second, it is not clear whether our result depends on the choice of the initial stabilizer pure state $|S\rangle$: Although we have observed that the late-time maximum of $M(e^{-iHt}|S\rangle\langle S|e^{iHt})$ is almost independent of the choice of $|S\rangle$, for the growth coefficient $a(L)$ it is still not clear at $L = 4$, where we have the results for a moderate variety of $|S\rangle$, whether $a(L)$ tends to be independent of $|S\rangle$ as L increases. It would be an important future direction to clarify these points.

2. Numerical supporting evidence: Stabilizer Rényi entropy

As the size of the system increases, the early-time behavior and saturation time of magic should become less dependent on finite size effects. However, it is difficult to study numerically the time evolution of mana in larger systems. Therefore, instead of mana, we consider here another magic monotone, the stabilizer Rényi entropy [28], which is defined for qubit systems ($d = 2$) and can be numerically computed on systems of larger sizes. We expect the stabilizer Rényi entropy to capture the early-time property of magic of the pure states.

For a pure state $|\psi\rangle$, the stabilizer Rényi entropy $M_2(|\psi\rangle)$ is defined as

$$M_2(|\psi\rangle) = -\log \sum_{P\in\bar{P}} (\Xi_P(|\psi\rangle))^2 - L\log 2, \tag{5.5}$$

[16]Note that the values of a may depend on the choice of the initial stabilizer pure state $|S\rangle$. Here we have chosen a particular set of stabilizer pure states that depend on L in a simple way.

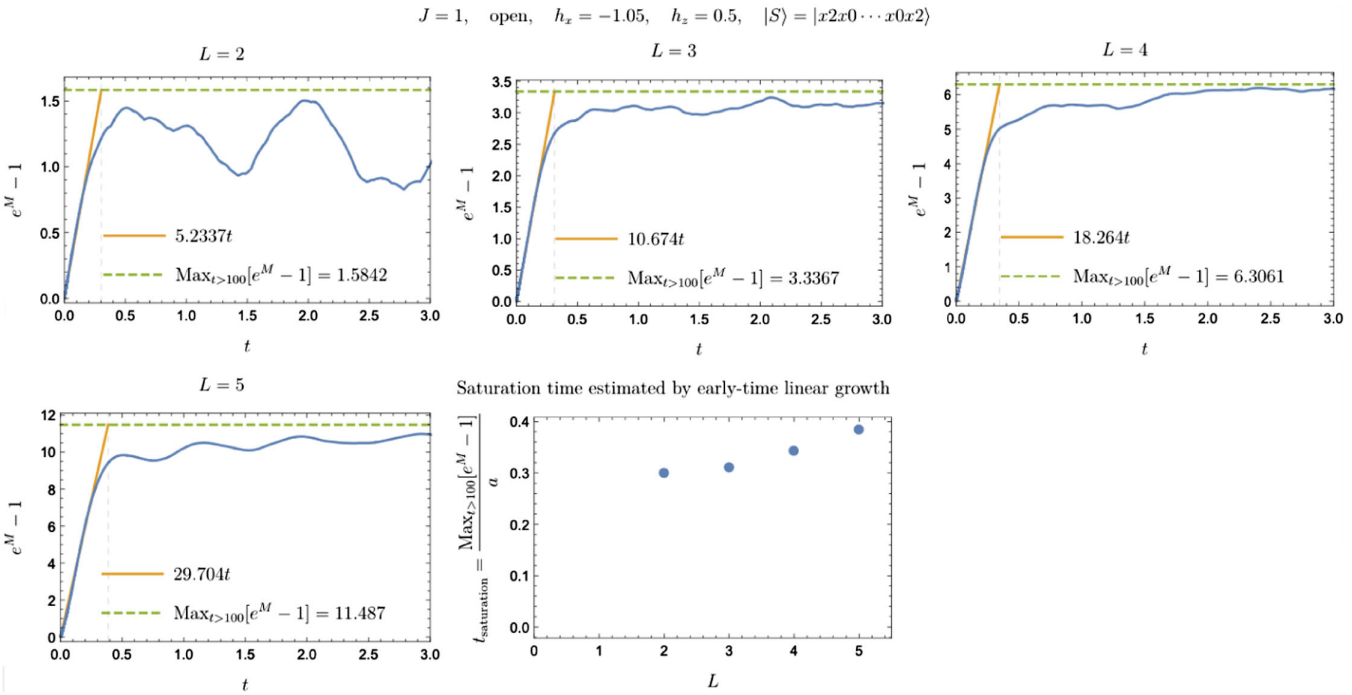

FIG. 8. First four panels: comparison between M and its maximum value at late times ($t > 100$) (dashed green line) with the early-time fitting with $e^M - 1 = at$ (orange line). Last panel: L dependence of the saturation time estimated by the early-time linear growth (vertical dashed lines in the other panels).

where[17] $\tilde{P}$ is the Pauli group divided by the overall phase: $\tilde{P} = \{1, z, x, izx\}^{\otimes L}$ with x, z given in (2.1), and

$$\Xi_P(|\psi\rangle) = \frac{1}{2^L}(\langle\psi|P|\psi\rangle)^2. \tag{5.7}$$

This $M_2(|\psi\rangle)$ satisfies the same properties as mana for $d \geq 3$: $M_2(|\psi\rangle) = M_2(U|\psi\rangle)$ for any pure state $|\psi\rangle$ and Clifford gate $U \in C_{d=2}$; $M_2(|\psi\rangle) = 0$ if and only if $|\psi\rangle \in \{|S\rangle\}$ (2.16); hence $M_2(|\psi\rangle)$ can be used as a magic monotone. Also note that $M_2(|\psi\rangle)$ is much easier to compute than robustness of magic (2.28) since $M_2(|\psi\rangle)$ does not involve any optimization procedure.

We analyze the time evolution of $M_2(e^{-iHt}|S\rangle)$, where $|S\rangle$ is one of the stabilizer pure states, which we have chosen as $|S\rangle = |x = -1\rangle \otimes |x = 1\rangle^{\otimes(L-2)} \otimes |x = -1\rangle$, for the open Ising model (3.1) at a chaotic point $(h_x, h_z) = (-1.05, 0.5)$ and two integrable points $(h_x, h_z) = (0, \sqrt{2}), (\sqrt{2}, 0)$. As a result, we obtain Fig. 9. In the chaotic case, $M_2(e^{-iHt}|S\rangle)$ grows monotonically at early times and oscillates at late times around some finite value proportional to L. We also find that as L increases, the magnitude of the late-time fluctuation of M_2 is more suppressed. On the other hand, in both of the integrable cases we find that M_2 comes back to $M_2 \approx 0$, the initial value, even at late times. Hence, our results suggest that the magic can distinguish the time evolution in chaotic systems from the time evolution in integrable systems, which is not clear in the analysis of robustness of magic due to the restriction to the small system size L. Thus, the stabilizer Rényi entropy can capture the same properties of magic as mana and RoM.

As we did for mana in Sec. V, we may also estimate the saturation time of $M_2(e^{-iHt}|S\rangle)$ at chaotic points as follows. We find that[18] at an early-time interval, $0.7 \leq t \leq 1$, $\sqrt{e^{M_2(e^{-iHt}|S\rangle)} - 1}$ grows linearly in t, $\sqrt{e^{M_2(e^{-iHt}|S\rangle)} - 1} \approx a'(L)t$, which we use to define the saturation time of M_2 as

$$t'_{\mathrm{saturation}} = \frac{\sqrt{e^{\max_{t>100}[M_2(e^{-iHt}|S\rangle)]} - 1}}{a'}. \tag{5.8}$$

[17]We can also consider the following generalization [28]:

$$M_2(|\psi\rangle) = (1-\alpha)^{-1} \log \sum_{P\in\tilde{P}} (\Xi_P(|\psi\rangle))^\alpha - L\log 2. \tag{5.6}$$

However, in this paper we focus on the case $\alpha = 2$ for simplicity.

[18]Here we consider $\sqrt{e^{M_2} - 1}$ instead of $e^{M_2} - 1$ by taking into account the fact that when we consider a state slightly deviated from a stabilizer pure state, the effect of deviation in M_2 vanishes at the first order.

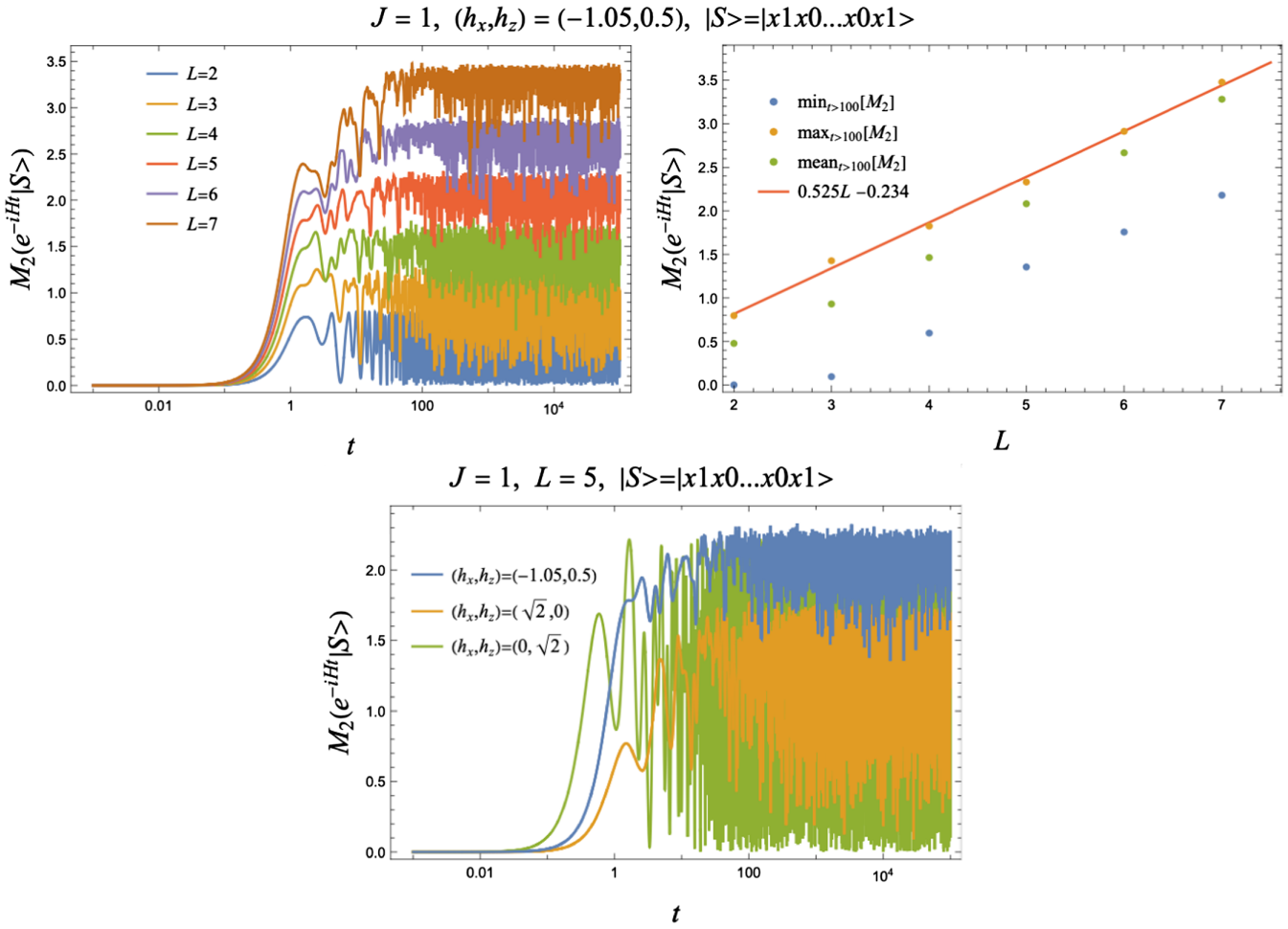

FIG. 9. Top: stabilizer Rényi entropy $M_2(e^{-iHt}|S\rangle)$ (top left) and its late-time values (top right) of the open Ising model (3.1) with $(h_x, h_z) = (-1.05, 0.5)$ for various values of L. Bottom: comparison of stabilizer Rényi entropy $M_2(e^{-iHt}|S\rangle)$ at a chaotic point $(h_x, h_z) = (-1.05, 0.5)$ and integrable points $(h_x, h_z) = (\sqrt{2}, 0), (0, \sqrt{2})$.

In Fig. 10 we display a' obtained by fitting for $L = 2, 3, \ldots, 7$. We observe that a' scales in L as $a'(L) \sim L$.[19]

Combining this with the scaling of the late-time value $M_2 \sim L$, we conclude that $t'_{\text{saturation}}$ grows exponentially in L. The current analysis provides additional [and stronger compared to the analysis of mana where $L \leq 5$ (see Sec. (5.4) and below)] evidence that magic keeps growing even after the system thermalizes (which occurs at $t \sim L$) when the system size is sufficiently large. In the context of holography, our results suggest that magic of states might reflect some nontrivial information of the black hole interiors in the dual geometry.

3. Early-time growth and nonstabilizerness

As in (2.22) and (5.5), both mana and stabilizer Rényi entropy quantify the nonstabilizerness of the quantum state. In particular, when the deviation of the state from the stabilizer states is small, one can show that these monotones capture the deviation from the stabilizer state at the first and second orders, respectively. Therefore, the early-time evolution of $e^{M(\rho)} - 1$ and $\sqrt{e^{M_2(\rho)} - 1}$ and the late-time values of the quantities discussed above suggest that the nonstabilizerness of the state grows linearly in time and saturates at an exponentially large time in the system size.

VI. DISCUSSIONS AND FUTURE DIRECTIONS

In this work, we studied the time dependence of the two measures of magic, mana and RoM, in the higher-spin generalized Ising model in the integrable and chaotic regimes. We chose stabilizer states, which can be efficiently simulated on a classical computer, as initial states, and considered their time evolution under the Hamiltonian of the system. We found that in the chaotic regime, both mana and RoM increase monotonically and saturate after a sufficiently late time to some nonzero value independent

[19]Note that the values of a' may depend on the choice of the initial stabilizer pure state $|S\rangle$. Here we have chosen a particular set of stabilizer pure states that depend on L in a simple way.

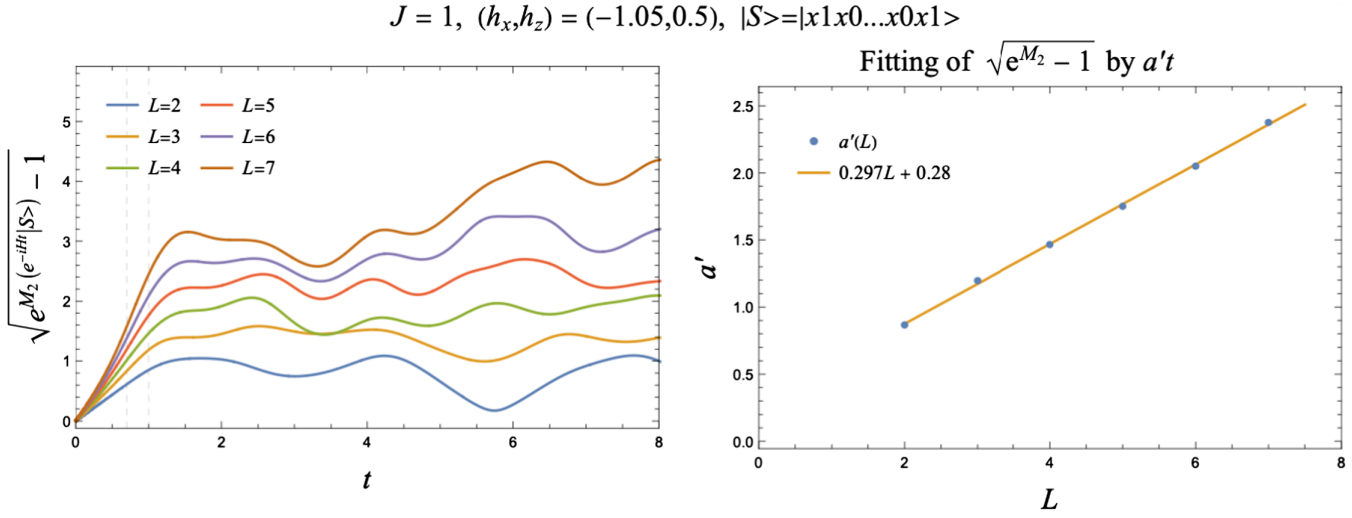

FIG. 10. Left: time evolution of $\sqrt{e^{M_2}-1}$. Right: rate of early-time linear growth of $\sqrt{e^{M_2}-1}$ obtained by fitting the data in the time interval $0.7 \le t \le 1$.

of the choices of an initial state and a boundary condition. In particular, mana at late times almost coincides with the optimal upper bound for a single-site system times the number of sites. This suggests that mana at late times almost saturates the optimal upper bound on mana for the entire Hilbert space. On the other hand, in the integrable regime, mana and RoM behave periodically in time, and the state transitions between low-magic and high-magic states. Our study suggests that magic of a quantum state is one of the key elements for the emergence of chaotic properties.

In this section, we list several further discussions and future directions.

(i) *Mana in a thermal state*

In this paper, we only focused on magic for a pure state. Here we make a brief comment on magic for a thermal state. Let us take the system of L sites, which has d degrees of freedom of the Hilbert space on each site; i.e., the dimension of the Hilbert space is d^L. We expect that the density matrix of a thermal state approximately takes the form

$$\rho_{\text{thermal}} \approx \frac{1}{d^L}\mathbb{1}, \tag{6.1}$$

where $\mathbb{1}$ is the $d^L \times d^L$ identity matrix. Computed from this density matrix, the Rényi entanglement entropy becomes independent of the replica index n. Jensen's inequality would suggest that mana is always zero. It would be intriguing to explore its physical interpretation.

(ii) *Mana in a mixed state*

Here we comment on the time evolution of mana for the mixed states in (2.17). Although mana is not a faithful magic monotone for mixed states, we think it is worth discussing the relation between the growth of magic and the entropy of the state. In the unitary nonequilibrium process, nth Rényi entropy is independent of time for any replica number n, while mana varies in time. The upper bound of mana is given by (2.23). In other words, the entropy of the mixed states inhibits the value of mana from growing in time.

(iii) *Mana for a subregion*

Mana studied in this paper is defined through the density matrix of a quantum state. We can simply generalize it to mana for a subregion using the *reduced* density matrix. Let us consider a state defined on L sites and divide the system into A with l_A sites and B with the remaining sites. We also assume that the size dependence of the Rényi entanglement entropy follows the Page curve [56,57]; i.e., the subsystem size dependence of the Rényi entanglement entropy $S_A^{(2)}$ for the region A is given by

$$S_A^{(2)} = \begin{cases} l_A \log d & \frac{L}{2} > l_A \\ (L - l_A)\log d & L > l_A > \frac{L}{2}. \end{cases} \tag{6.2}$$

This suggests that the upper bound for the subsystem generalization of mana $\mathcal{M}_A$ defined by the reduced density matrix ρ_A is given by

$$\mathcal{M}_A \le \begin{cases} 0 & 0 < l_A < \frac{L}{2} \\ l_A - \frac{L}{2} & \frac{L}{2} < l_A < L. \end{cases} \tag{6.3}$$

It is worth noting that the subregion generalization of mana $\mathcal{M}_A$ is always 0 for a small subregion $0 < l < \frac{L}{2}$. It is known that the entanglement entropy in a thermofield double state in a two-dimensional holographic conformal field theory on a compact spacetime [58] and a chaotic chain [59] follows the Page curve at

sufficiently late times, and we expect the subregion generalization of mana will satisfy (6.3).[20]

An interesting future direction is to find the gravity dual of mana and RoM. It would be interesting to find the geometrical meaning of the maximally magical states, which would be realized in the holographic systems.

In our paper, we performed numerical computations for mana and RoM, but there would be some subtleties due to the small system size. It would be interesting to study them for larger systems. Such a direction is important to find their gravity dual.

It is important to define mana and RoM in a continuous quantum field theory and study their time dependence.

In Sec. II B we observed that under chaotic dynamics, any state evolves to some state $|\psi(t)\rangle$ whose mana is $M(|\psi(t)\rangle\langle\psi(t)|) \approx LM_0(d,1)$, where L is the number of sites, d is the dimension of the single-site Hilbert space, and $M_0(d,1)$ is the optimal upper bound on mana of the single-site system, at least for $d = 3$. One possible choice of state to reproduce the same amount of mana is

$$U \bigotimes_{i=1}^{L} |m_i\rangle, \tag{6.4}$$

with each $|m_i\rangle$ being one of the states in the single-site system whose mana saturates $M = M_0(d,1)$, and U some element of the Clifford group C_d of the L-site system. Such single-site states $|m\rangle$ are known concretely for $d = 3$, 5 [35,37]. It would be interesting to study whether the late-time state can be expressed in the form (6.4),[21] or more generally, whether the state at early times where mana is still growing can also be expressed in a similar form: $U(t)(\otimes_i^{\ell(t)} |m_i\rangle \otimes |S\rangle)$ with $\ell(t) \approx M(|\psi\rangle\langle\psi|)/M_0(d,1)$ and $|S\rangle$ some stabilizer state in the $L - \ell(t)$-site system. Conversely, it would also be interesting to study whether dynamics under which any state evolves to an almost maximally magical state is always strongly chaotic.

ACKNOWLEDGMENTS

We thank Shinsei Ryu, Kotaro Tamaoka, and Tadashi Takayanagi for valuable discussions. We thank Tomoyuki Morimae for an introductory seminar on the basics of magic at YITP, Kyoto University. K. G. is supported by JSPS Grant-in-Aid for Early-Career Scientists No. 21K13930. M. N. is supported by JSPS Grant-in-Aid for Early-Career Scientists No. 19K14724. The numerical results were obtained using the high-performance computing facilities provided at SISSA (Ulysses) and at the Yukawa Institute for Theoretical Physics (Sushiki server).

APPENDIX A: INITIAL-STATE DEPENDENCE OF MANA AND ROM

In this appendix, we display the results on the dependence of mana $M(\rho)$ and RoM(ρ) for $\rho = e^{-iHt}|S\rangle\langle S|e^{iHt}$ on the choice of the initial state $|S\rangle$. For simplicity, we display only the numerically realized values of the maximum and minimum at late times ($100 < t < 10^5$). We also omit the results for the trivially integrable ($h_x = 0$) cases. In Tables I and II, we list the results for mana with $j = 1$, $L = 4$, where we have selected only part of the stabilizer states for $|S\rangle$ among the full set of stabilizer pure states, which consists of 7439040 (2.16), while in Figs. 11 and 12, we display the

TABLE I. Observed maximum and minimum values of $M(e^{-iHt}|S\rangle\langle S|e^{iHt})$ for $L = 4$, $(j, h_x, h_z) = (1, -1.05, 0.5)$ with $t > 100$. As the initial states $|S\rangle$, we have chosen those in the form $|I_1 n_1\rangle \otimes |I_2 n_2\rangle \otimes \cdots |I_L n_L\rangle$ with $|In\rangle$ the eigenstate of I with eigenvalue ω^n ($I = x, z$; $n = 0, 1, \ldots, d$), which we have abbreviated as $|I_1 n_1 I_2 n_2 \cdots I_L n_L\rangle$.

	$h_x = -1.05$, $h_z = 0.5$, open		$h_x = -1.05$, $h_z = 0.5$, periodic	
$\|S\rangle$	$\mathrm{Max}_{t>100}$ $[M]$	$\mathrm{Min}_{t>100}$ $[M]$	$\mathrm{Max}_{t>100}$ $[M]$	$\mathrm{Min}_{t>100}$ $[M]$
$\|x0x0x0x0\rangle$	1.94848	1.5446	1.9677	1.35928
$\|x0x1x1x0\rangle$	1.98867	1.92726	1.98738	1.90887
$\|x0x2x2x0\rangle$	1.98872	1.94041	1.98788	1.88011
$\|x0z0z0x0\rangle$	1.98775	1.94232	1.98697	1.93669
$\|x0z1z1x0\rangle$	1.98389	1.8928	1.98385	1.84364
$\|x0z2z2x0\rangle$	1.98663	1.8807	1.98492	1.84096
$\|x1x0x0x1\rangle$	1.98809	1.93112	1.98738	1.90887
$\|x1x1x1x1\rangle$	1.98658	1.83597	1.99177	1.71701
$\|x1x2x2x1\rangle$	1.98586	1.90739	1.98814	1.87717
$\|x1z0z0x1\rangle$	1.9799	1.83753	1.98052	1.85992
$\|x1z1z1x1\rangle$	1.98999	1.93231	1.9873	1.92717
$\|x1z2z2x1\rangle$	1.9897	1.9217	1.99008	1.91503
$\|x2x0x0x2\rangle$	1.98636	1.94038	1.98788	1.88011
$\|x2x1x1x2\rangle$	1.98448	1.92106	1.98814	1.87717
$\|x2x2x2x2\rangle$	1.98384	1.87289	1.9886	1.71676
$\|x2z0z0x2\rangle$	1.97987	1.82827	1.98082	1.85984
$\|x2z1z1x2\rangle$	1.98799	1.93234	1.99067	1.9296
$\|x2z2z2x2\rangle$	1.99014	1.91262	1.99007	1.91344
$\|z0x0x0z0\rangle$	1.98726	1.93525	1.98697	1.93669
$\|z0x1x1z0\rangle$	1.9862	1.91971	1.98052	1.85992
$\|z0x2x2z0\rangle$	1.98632	1.92497	1.98082	1.85984
$\|z1x0x0z1\rangle$	1.98368	1.86783	1.98385	1.84364
$\|z1x1x1z1\rangle$	1.98894	1.94228	1.9873	1.92717
$\|z1x2x2z1\rangle$	1.98769	1.94325	1.99067	1.9296
$\|z2x0x0z2\rangle$	1.97872	1.71465	1.98492	1.84096
$\|z2x1x1z2\rangle$	1.9875	1.92687	1.99008	1.91503
$\|z2x2x2z2\rangle$	1.98956	1.91078	1.99007	1.91344

[20]Since the time evolution of the Rényi entanglement entropy in a two-dimensional holographic conformal field theory depends on the Rényi index, a correction to (6.3) may be necessary.

[21]Note that the state $\otimes_{i=1}^{L} |m_i\rangle$ does not have any entanglement. If a late-time state is of the form (6.4), the large entanglement of the state, which is a characteristic of chaotic dynamics, should be carried by the choice of U.

TABLE II. Observed maximum and minimum values of $M(e^{-iHt}|S\rangle\langle S|e^{iHt})$ for $L=4$, $(j,h_x,h_z)=(1,1,0)$ with $t>100$.

	$h_x=1$, $h_z=0$, open		$h_x=1$, $h_z=0$, periodic	
$\|S\rangle$	$\mathrm{Max}_{t>100}[M]$	$\mathrm{Min}_{t>100}[M]$	$\mathrm{Max}_{t>100}[M]$	$\mathrm{Min}_{t>100}[M]$
$\|x0x0x0x0\rangle$	1.95063	1.19597	1.97313	1.02994
$\|x0x1x1x0\rangle$	1.98697	1.85128	1.98538	1.80405
$\|x0x2x2x0\rangle$	1.98697	1.85128	1.98538	1.80405
$\|x0z0z0x0\rangle$	1.97238	1.74603	1.97888	1.65442
$\|x0z1z1x0\rangle$	1.99427	1.73786	1.99098	1.63055
$\|x0z2z2x0\rangle$	1.97238	1.74603	1.97888	1.65442
$\|x1x0x0x1\rangle$	1.98562	1.92734	1.98538	1.80405
$\|x1x1x1x1\rangle$	1.98471	1.68569	1.99113	1.47506
$\|x1x2x2x1\rangle$	1.98424	1.85524	1.98713	1.54085
$\|x1z0z0x1\rangle$	1.98772	1.93549	1.98578	1.8906
$\|x1z1z1x1\rangle$	1.98519	1.88945	1.98748	1.91064
$\|x1z2z2x1\rangle$	1.99302	1.94148	1.98737	1.90967
$\|x2x0x0x2\rangle$	1.98562	1.92734	1.98538	1.80405
$\|x2x1x1x2\rangle$	1.98424	1.85524	1.98713	1.54085
$\|x2x2x2x2\rangle$	1.98471	1.68569	1.99113	1.47506
$\|x2z0z0x2\rangle$	1.99302	1.94148	1.98737	1.90967
$\|x2z1z1x2\rangle$	1.98519	1.88945	1.98748	1.91064
$\|x2z2z2x2\rangle$	1.98772	1.93549	1.98578	1.8906
$\|z0x0x0z0\rangle$	1.98424	1.78507	1.97888	1.65442
$\|z0x1x1z0\rangle$	1.98727	1.91742	1.98578	1.8906
$\|z0x2x2z0\rangle$	1.98719	1.91027	1.98737	1.90967
$\|z1x0x0z1\rangle$	1.99068	1.77276	1.99098	1.63055
$\|z1x1x1z1\rangle$	1.98859	1.90417	1.98748	1.91064
$\|z1x2x2z1\rangle$	1.98859	1.90417	1.98748	1.91064
$\|z2x0x0z2\rangle$	1.98424	1.78507	1.97888	1.65442
$\|z2x1x1z2\rangle$	1.98719	1.91027	1.98737	1.90967
$\|z2x2x2z2\rangle$	1.98727	1.91742	1.98578	1.8906

results for RoM with $j=1/2, L=3$ and $j=1, L=2$ for all stabilizer states $|S\rangle$.

APPENDIX B: INITIAL TIME BEHAVIOR OF MANA

In this section we display some analysis on the initial time linear growth of mana $M(e^{-iHt}|S\rangle\langle S|e^{iHt})$ which we observed in Sec. V. First we observe that a stabilizer pure state $|S\rangle=|0\rangle^{\otimes L}$ and the phase space point operators have the following properties[22]:

$$A_{\vec{a}}|S\rangle=|S\rangle \text{ for some } d^L \text{ choices of } \vec{a}. \tag{B1}$$

$$A\langle S|A_{\vec{a}}|S\rangle=0 \text{ for all other } d^{2L}-d^L \text{ choices of } \vec{a}. \tag{B2}$$

Now let us consider the initial time approximation of $e^{M(\rho(t))}$ with $\rho(t)=e^{-iHt}|S\rangle\langle S|e^{iHt}$. At the second order in the small t expansion, $\rho(t)$ is given by

$$\rho(t)=|S\rangle\langle S|-it[H,|S\rangle\langle S|]+\mathcal{O}(t^2). \tag{B3}$$

Then, $e^{M(\rho(t))}$ at the second order of the small t expansion is given by

$$e^{M(\rho(t))}=\frac{1}{d^L}\sum_{\vec{a}}|\langle S|A_{\vec{a}}|S\rangle+it\langle S|[H,A_{\vec{a}}]|S\rangle|+\mathcal{O}(t^2). \tag{B4}$$

Thus, in the small t expansion, the time evolution of $e^{M(\rho(t))}$ is determined by the time evolution of phase space point operators. By using the above observation, we can rewrite this as

$$e^{M(\rho(t))}=1+a_{\mathrm{small}\,t}t+\mathcal{O}(t^2), \tag{B5}$$

with

$$a_{\mathrm{small}\,t}=\frac{1}{d^L}\sum_{\vec{a}}|\langle S|[H,A_{\vec{a}}]|S\rangle|. \tag{B6}$$

We can obtain a relatively simple pair of upper and lower bounds of $a_{\mathrm{small}\,t}$. For this purpose we use the following inequality:

$$\sqrt{\sum_{i=1}^{n}|c_i|^2}\le\sum_{i=1}^{n}|c_i|\le\sqrt{n\sum_{i=1}^{n}|c_i|^2}, \tag{B7}$$

which holds for any complex numbers $c_1,\ldots,c_n$. Here the first inequality is obvious, while the second inequality follows from the concavity of the function $f(x)=\sqrt{x}$. Applying (B7) to $a_{\mathrm{small}\,t}$ in (B6), we obtain

$$a^{(\mathrm{lower})}_{\mathrm{small}\,t}\le a_{\mathrm{small}\,t}\le d^L a^{(\mathrm{lower})}_{\mathrm{small}\,t}, \tag{B8}$$

with

$$a^{(\mathrm{lower})}_{\mathrm{small}\,t}=\frac{1}{d^L}\sqrt{\sum_{\vec{a}}|\langle S|[H,A_{\vec{a}}]|S\rangle|^2}. \tag{B9}$$

By using the identity $\sum_{\vec{a}}(A_{\vec{a}})_{ij}(A_{\vec{a}})_{k\ell}=d^L\delta_{i\ell}\delta_{jk}$, which follows since $\{A_{\vec{a}}\}$ is an orthonormal basis set, we can simplify $a^{(\mathrm{lower})}_{\mathrm{small}\,t}$ as

$$a^{(\mathrm{lower})}_{\mathrm{small}\,t}=d^{-\frac{L}{2}}\sqrt{2(\langle S|H^2|S\rangle-(\langle S|H|S\rangle)^2)}. \tag{B10}$$

[22]For $|S\rangle=|0\rangle^{\otimes L}$ we can show by direct calculations that (B2) holds where the first d^L choices of $\vec{a}$ are $\{((a_1,0),(a_2,0),\ldots,(a_L,0))\}$. We have confirmed (B2) also holds with all the other stabilizer pure states $|S\rangle$ for $d=3, L=1$, 2 and with a large number of stabilizer pure states for $d=3$, $L=3$.

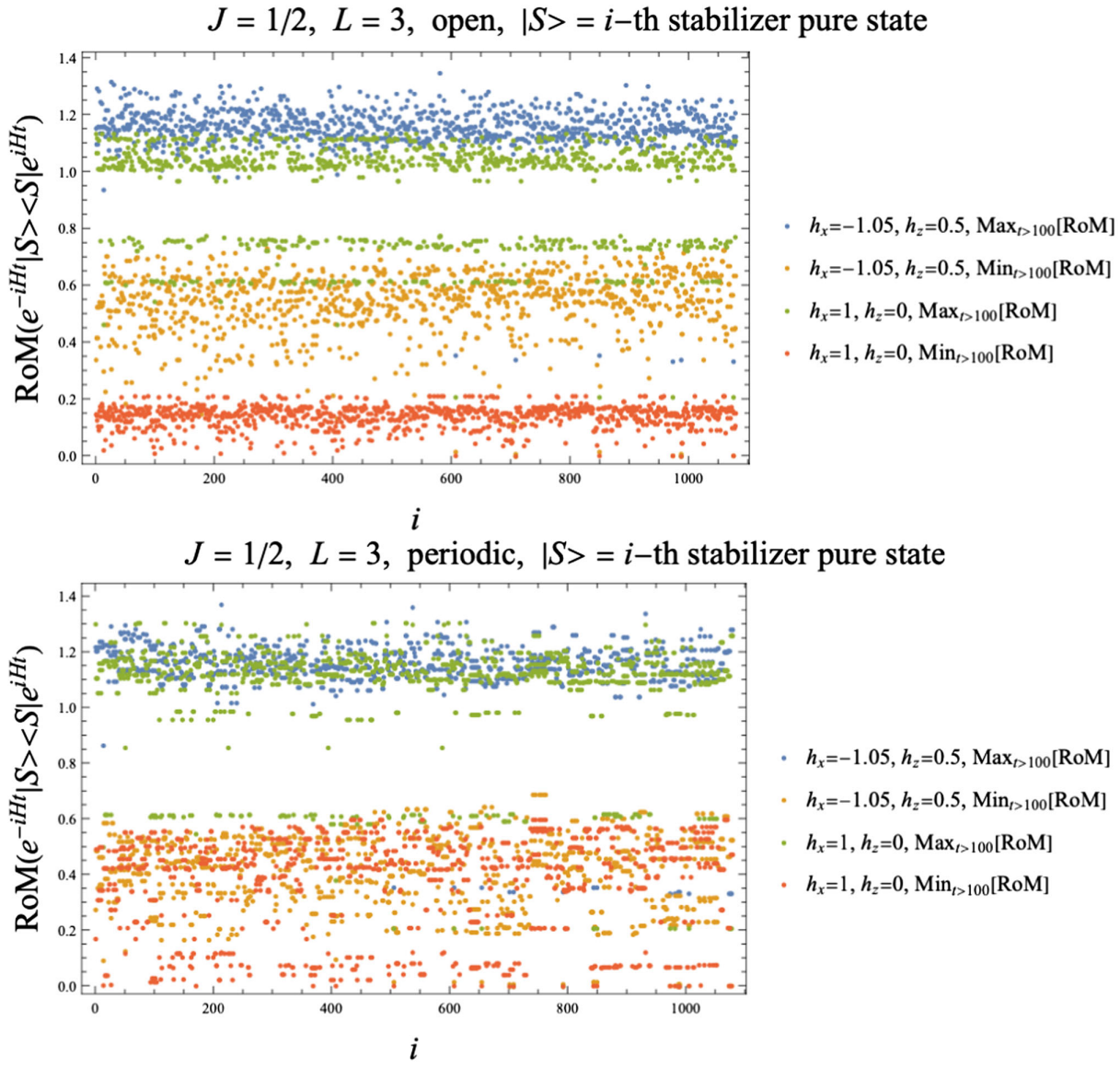

FIG. 11. Observed maximum and minimum values of $\mathrm{RoM}(e^{-iHt}|S\rangle\langle S|e^{iHt})$ for $L=3$, $(j,h_x,h_z)=(1/2,-1.05,0.5)$ and $(j,h_x,h_z)=(1/2,1,0)$ with $t>100$. The horizontal axis indicates that the ith stabilizer pure state among all 1080 stabilizer pure states is chosen as the initial state $|S\rangle$.

Hence we obtain

$$d^{-\frac{L}{2}}\sqrt{2(\langle S|H^2|S\rangle-(\langle S|H|S\rangle)^2)}\le a_{\mathrm{small}\,t}\le d^{\frac{L}{2}}\sqrt{2(\langle S|H^2|S\rangle-(\langle S|H|S\rangle)^2)}. \tag{B11}$$

Note that the upper and lower bounds of $a_{\mathrm{small}\,t}$ are much easier to evaluate than $a_{\mathrm{small}\,t}$ itself.

However, at least for the chaotic Ising model with $d=3, L=2,\ 3$, we find that neither the lower bound nor the upper bound is close to the actual value of $a_{\mathrm{small}\,t}$. Moreover, for the same model we find that $a_{\mathrm{small}\,t}$ itself is not close to the slope of the wide linear growth regime considered in Sec. V either (except for $L=3$; see Fig. 13). Indeed, the small t expansion in this section is based on the assumption that $e^M-1\ll 1$ and hence may not be reliable in the regime where mana approaches an exponentially large late time value. It would be interesting to study whether there is a chaotic system where these situations are different.

APPENDIX C: COMPARISON BETWEEN ENTANGLEMENT AND MAGIC MONOTONES

In this section we compare the magic of the time-evolved states $e^{-iHt}|S\rangle$ with the entanglement of the same states in the chaotic parameter regime $(h_x,h_z)=(-1.05,0.5)$. As a measure of the entanglement, here we adopt the entanglement entropy S_A with A

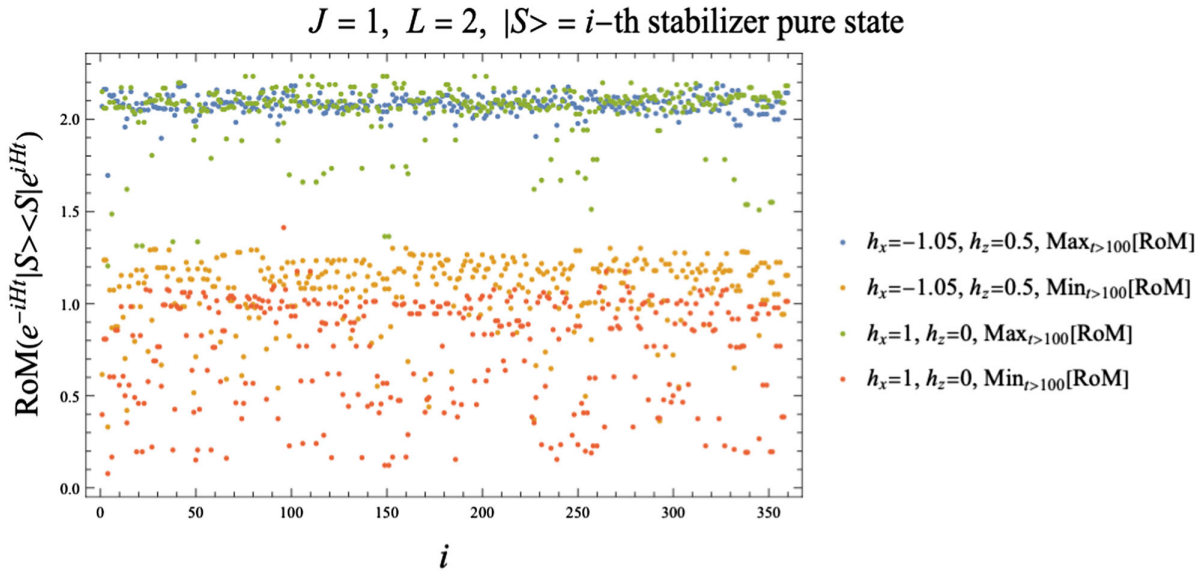

FIG. 12. Observed maximum and minimum values of $\mathrm{RoM}(e^{-iHt}|S\rangle\langle S|e^{iHt})$ for $L = 2$, $(j, h_x, h_z) = (1, -1.05, 0.5)$ and $(j, h_x, h_z) = (1, 1, 0)$ with $t > 100$. The horizontal axis indicates that the ith stabilizer pure state among all 360 stabilizer pure states is chosen as the initial state $|S\rangle$.

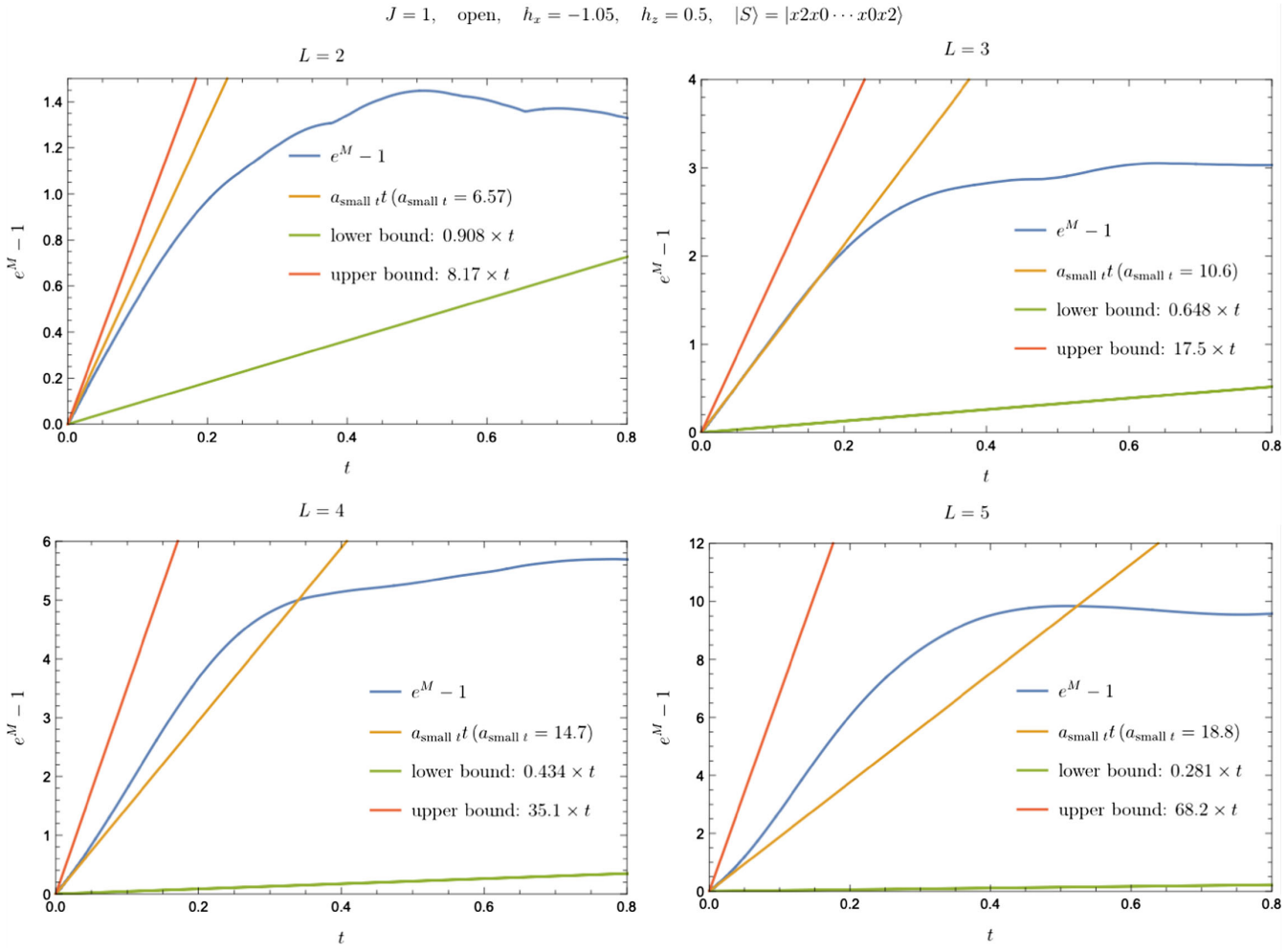

FIG. 13. Comparison between the leading coefficient $a_{\mathrm{small}\,t}$ of the initial time expansion (B9), the simpler upper and lower bounds of $a_{\mathrm{small}\,t}$, and the actual values of mana for the higher-spin generalized open Ising model (3.1) with $(J, h_x, h_z) = (1, -1.05, 0.5)$ and $L = 2, 3, 4, 5$.

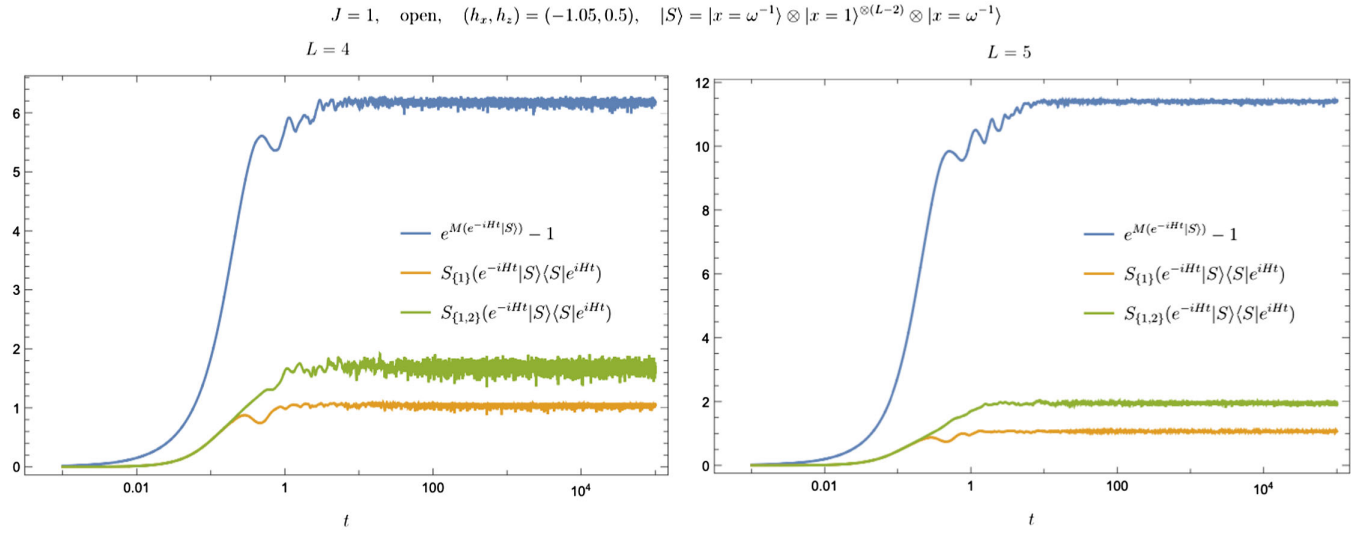

FIG. 14. Comparison between mana and the entanglement entropy for $|S\rangle = |x = \omega^{-1}\rangle \otimes |x = 1\rangle^{\otimes(L-2)} \otimes |x = \omega^{-1}\rangle$, in the chaotic regime $(h_x, h_z) = (-1.05, 0.5)$.

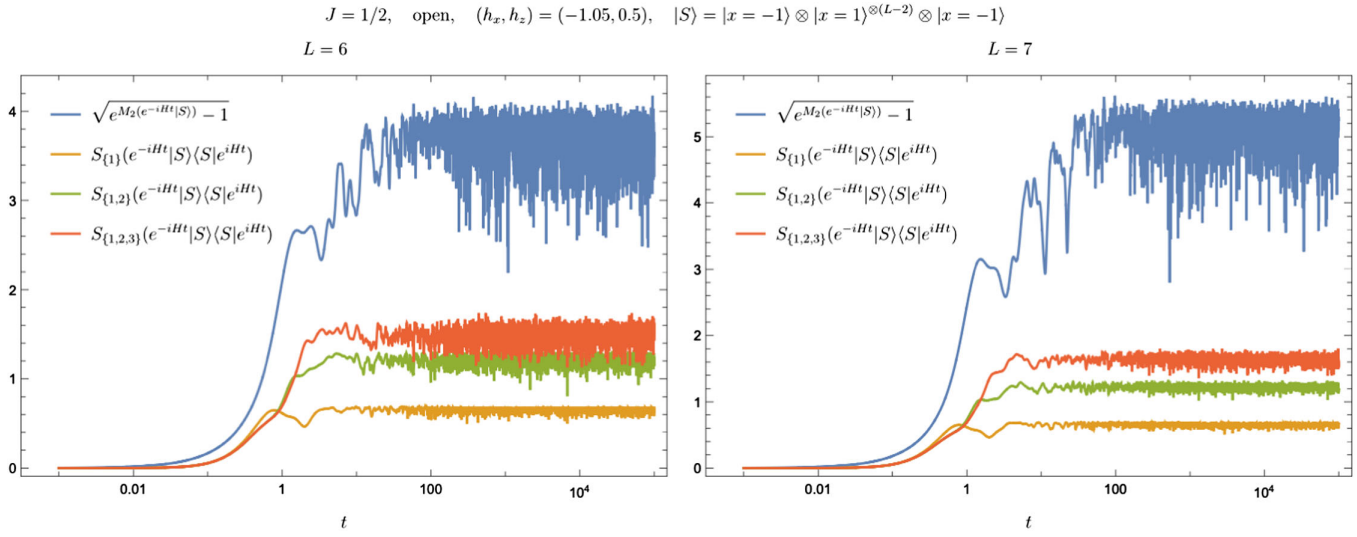

FIG. 15. Comparison between the stabilizer Rényi entropy and the entanglement entropy for $|S\rangle = |x = -1\rangle \otimes |x = 1\rangle^{\otimes(L-2)} \otimes |x = -1\rangle$, in the chaotic regime $(h_x, h_z) = (-1.05, 0.5)$.

chosen as the first ℓ sites of the spin chain ($1 \le \ell \le [\frac{L}{2}]$). We are particularly interested in the cases where L is large; hence, here we consider only mana for $J = 1$ ($d = 3$) and the stabilizer Rényi entropy for $J = 1/2$ ($d = 2$), which are tractable for relatively larger L compared with the robustness of magic, as the measures of magic. We also focus only on the spin chains with the open boundary condition for simplicity.

When the initial stabilizer state is chosen as $|S\rangle = |x = \omega^{-1}\rangle \otimes |x = 1\rangle^{\otimes(L-2)} \otimes |x = \omega^{-1}\rangle$, we obtain Figs. 14 and 15. From these results we find that the behaviors of the magic monotones are slightly different from the behavior of the entanglement entropy. Interestingly, we also observe that the magic monotone keeps increasing even after the entanglement entropy saturates.[23]

[23]Note, however, that this postscrambling growth of magic is observed to take place in a different time region ($1 \lesssim t \lesssim 10$ for mana with $L = 4$, 5 and $1 \lesssim t \lesssim 100$ for the stabilizer Rényi entropy with $L = 6$, 7) from the time region we focused on to estimate the saturation time of magic ($0.1 \le t \le 0.2$ for mana and $0.7 \le t \le 1$ for the stabilizer Rényi entropy) in Sec. V. We hope to revisit the postscrambling behavior of the magic monotones, together with a more reasonable estimation of the saturation time, in future analyses.

APPENDIX D: TIME EVOLUTION OF MAGIC FROM HIGHLY ENTANGLED STABILIZER STATE

In Secs. IV and V, we studied the time evolution of the magic monotones from a tensor product stabilizer pure state and found that the behavior of the magic monotones in the chaotic regime is qualitatively different from the behavior in the integrable regime. Note, however, that the behavior of the entanglement entropy is also qualitatively different in the chaotic regime and in the integrable regime for this setup: The entanglement entropy grows to the maximum value $S_A \sim |A| \log d$ only when the system is chaotic. Therefore, from the results in this setup, it is not clear whether the difference of the behavior of magic really reflects the chaoticity of the Hamiltonian or whether it just reflects the entanglement property of the state. In this appendix, in order to separate the behavior of the magic monotones from the entanglement, we study the time evolution from the following initial state:

$$|S\rangle = \begin{cases} |B\rangle_{1,L} \otimes |B\rangle_{2,L-1} \otimes \cdots \otimes |B\rangle_{\frac{L}{2},\frac{L}{2}+1} & L: \text{ even} \\ |B\rangle_{1,L} \otimes |B\rangle_{2,L-1} \otimes \cdots \otimes |B\rangle_{[\frac{L}{2}],[\frac{L}{2}]+2} \otimes |x=1\rangle_{[\frac{L}{2}]+1} & L: \text{ odd}, \end{cases} \tag{D1}$$

where $|B\rangle_{i,j} = \frac{1}{\sqrt{2J+1}} \sum_{n=0}^{2J} |x=\omega^n\rangle_i \otimes |x=\omega^n\rangle_j$ is a Bell pair between the ith and jth sites. For example, for $J = 1/2, L = 4$, Eq. (D1) reduces to

$$\begin{aligned} |S\rangle = \frac{1}{2}(&|x=1\rangle \otimes |x=1\rangle \otimes |x=1\rangle \otimes |x=1\rangle + |x=1\rangle \otimes |x=-1\rangle \otimes |x=-1\rangle \otimes |x=1\rangle \\ &+ |x=-1\rangle \otimes |x=1\rangle \otimes |x=1\rangle \otimes |x=-1\rangle + |x=-1\rangle \otimes |x=-1\rangle \otimes |x=-1\rangle \otimes |x=-1\rangle). \end{aligned} \tag{D2}$$

Note that $|S\rangle$ in (D1) is a stabilizer pure state, although it is maximally entangled between $A = \{1, 2, \ldots, [\frac{L}{2}]\}$ and its complement. In this setup we obtain the results displayed in Figs. 16 and 17. We find that mana in the chaotic regime deviates from mana in the integrable regime, and at late times, we find that the integrable case shows a smaller saturation value and larger fluctuation compared with the chaotic case. We find the same discrepancy between the stabilizer Rényi entropy in the chaotic regime and the stabilizer Rényi entropy in both of the integrable regimes when t is not too small (say, $t \gtrsim 0.3$). These results suggest that magic indeed distinguishes a chaotic dynamics from an integrable dynamics in a different manner than the entanglement does.

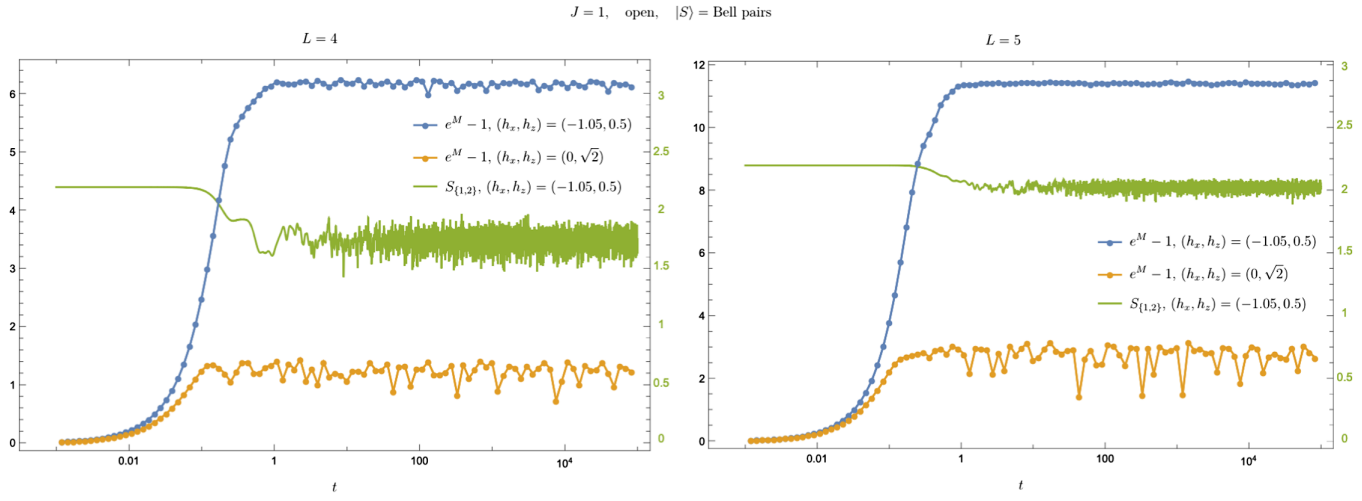

FIG. 16. Mana $M(e^{-iHt}|S\rangle)$ in the chaotic regime and integrable regime for $|S\rangle$ being the Bell pair state (D1). Note that the apparently small fluctuation of $e^M - 1$ in the integrable regime at late times is simply due to the small number of discrete data points. For comparison, we also display the entanglement entropy $S_{\{1,2\}}$ in the chaotic regime. Here, values of $e^M - 1$ are indicated with the left tick marks while the values of $S_{\{1,2\}}$ are indicated with the right tick marks.

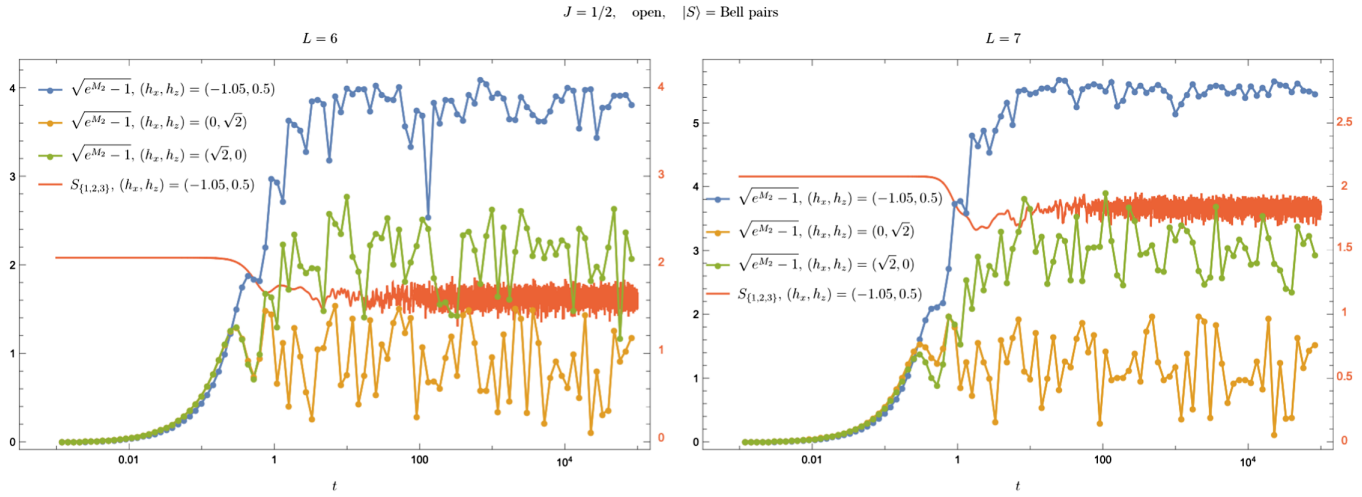

FIG. 17. Robustness of magic $M_2(e^{-iHt}|S\rangle)$ in the chaotic regime and integrable regime for $|S\rangle$ being the Bell pair state (D1). For comparison, we also display the entanglement entropy $S_{\{1,2,3\}}$ in the chaotic regime. Here, values of $\sqrt{e^{M_2}-1}$ are indicated with the left ticks while the values of $S_{\{1,2\}}$ are indicated with the right ticks.

[1] J. Maldacena, The large-N limit of superconformal field theories and supergravity, Int. J. Theor. Phys. **38**, 1113 (1999).
[2] S. Gubser, I. Klebanov, and A. Polyakov, Gauge theory correlators from non-critical string theory, Phys. Lett. B **428**, 105 (1998).
[3] E. Witten, Anti-de Sitter space and holography, Adv. Theor. Math. Phys. **2**, 253 (1998).
[4] S. Ryu and T. Takayanagi, Holographic Derivation of Entanglement Entropy from the anti de Sitter Space/Conformal Field Theory Correspondence, Phys. Rev. Lett. **96**, 181602 (2006).
[5] L. Susskind, Entanglement is not enough, Fortschr. Phys. **64**, 49 (2016).
[6] C. D. White, C. Cao, and B. Swingle, Conformal field theories are magical, Phys. Rev. B **103**, 075145 (2021).
[7] T. Hartman and J. Maldacena, Time evolution of entanglement entropy from black hole interiors, J. High Energy Phys. 05 (2013) 014.
[8] M. A. Nielsen, A geometric approach to quantum circuit lower bounds, arXiv:quant–ph/0502070.
[9] M. A. Nielsen, M. R. Dowling, M. Gu, and A. C. Doherty, Quantum computation as geometry, Science **311**, 1133 (2006).
[10] M. R. Dowling and M. A. Nielsen, The geometry of quantum computation, arXiv:quant–ph/0701004.
[11] L. Susskind, Computational complexity and black hole horizons, Fortschr. Phys. **64**, 24 (2016); **64**, 44(A) (2016).
[12] A. R. Brown, D. A. Roberts, L. Susskind, B. Swingle, and Y. Zhao, Holographic Complexity Equals Bulk Action?, Phys. Rev. Lett. **116**, 191301 (2016).
[13] A. R. Brown, D. A. Roberts, L. Susskind, B. Swingle, and Y. Zhao, Complexity, action, and black holes, Phys. Rev. D **93**, 086006 (2016).
[14] K. Goto, H. Marrochio, R. C. Myers, L. Queimada, and B. Yoshida, Holographic complexity equals which action?, J. High Energy Phys. 02 (2019) 160.
[15] A. Belin, R. C. Myers, S.-M. Ruan, G. Sárosi, and A. J. Speranza, Does Complexity Equal Anything?, Phys. Rev. Lett. **128**, 081602 (2022).
[16] D. Gottesman, Stabilizer codes and quantum error correction, arXiv:quant-ph/9705052.
[17] D. Gottesman, The Heisenberg representation of quantum computers, in *Proceedings of the XXII International Colloquium on Group Theoretical Methods in Physics*, edited by S. P. Corney, R. Delbourgo, and P. D. Jarvis (International Press, Cambridge, MA, 1999), pp. 32–43.
[18] C. Chamon, A. Hamma, and E. R. Mucciolo, Emergent Irreversibility and Entanglement Spectrum Statistics, Phys. Rev. Lett. **112**, 240501 (2014).
[19] D. Shaffer, C. Chamon, A. Hamma, and E. R. Mucciolo, Irreversibility and entanglement spectrum statistics in quantum circuits, J. Stat. Mech. (2014) P12007.
[20] Z.-C. Yang, A. Hamma, S. M. Giampaolo, E. R. Mucciolo, and C. Chamon, Entanglement complexity in quantum many-body dynamics, thermalization, and localization, Phys. Rev. B **96**, 020408 (2017).
[21] S. Zhou, Z.-C. Yang, A. Hamma, and C. Chamon, Single T gate in a Clifford circuit drives transition to universal entanglement spectrum statistics, SciPost Phys. **9**, 87 (2020).

[22] J. R. Fliss, Knots, links, and long-range magic, J. High Energy Phys. 04 (2021) 090.
[23] X. Zhou, D. W. Leung, and I. L. Chuang, Methodology for quantum logic gate construction, Phys. Rev. A **62**, 052316 (2000).
[24] S. Bravyi, G. Smith, and J. A. Smolin, Trading Classical and Quantum Computational Resources, Phys. Rev. X **6**, 021043 (2016).
[25] S. Bravyi and D. Gosset, Improved Classical Simulation of Quantum Circuits Dominated by Clifford Gates, Phys. Rev. Lett. **116**, 250501 (2016).
[26] X. Wang, M. M. Wilde, and Y. Su, Quantifying the magic of quantum channels, New J. Phys. **21**, 103002 (2019).
[27] Z.-W. Liu and A. Winter, Many-body quantum magic, PRX Quantum **3**, 020333 (2022).
[28] L. Leone, S. F. E. Oliviero, and A. Hamma, Rényi Entropy of Magic, Phys. Rev. Lett. **128**, 050402 (2022).
[29] L. Leone, S. F. E. Oliviero, Y. Zhou, and A. Hamma, Quantum chaos is quantum, Quantum **5**, 453 (2021).
[30] L. Leone, S. F. E. Oliviero, and A. Hamma, Isospectral twirling and quantum chaos, Entropy **23**, 1073 (2021).
[31] B. Craps, M. De Clerck, D. Janssens, V. Luyten, and C. Rabideau, Lyapunov growth in quantum spin chains, Phys. Rev. B **101**, 174313 (2020).
[32] D. Gottesman, A theory of fault tolerant quantum computation, Phys. Rev. A **57**, 127 (1998).
[33] D. Gottesman, Fault tolerant quantum computation with higher-dimensional systems, Chaos Solitons Fractals **10**, 1749 (1999).
[34] D. Gross, Hudson's theorem for finite-dimensional quantum systems, J. Math. Phys. (N.Y.) **47**, 122107 (2006).
[35] V. Veitch, S. A. Hamed Mousavian, D. Gottesman, and J. Emerson, The resource theory of stabilizer quantum computation, New J. Phys. **16**, 013009 (2014).
[36] C. D. White and J. H. Wilson, Mana in Haar-random states, arXiv:2011.13937.
[37] A. Jain and S. Prakash, Qutrit and ququint magic states, Phys. Rev. A **102**, 042409 (2020).
[38] M. Howard and E. Campbell, Application of a Resource Theory for Magic States to Fault-Tolerant Quantum Computing, Phys. Rev. Lett. **118**, 090501 (2017).
[39] M. Ahmadi, H. B. Dang, G. Gour, and B. C. Sanders, Quantification and manipulation of magic states, Phys. Rev. A **97**, 062332 (2018).
[40] M. Heinrich and D. Gross, Robustness of magic and symmetries of the stabiliser polytope, Quantum **3**, 132 (2019).
[41] S. Sarkar, C. Mukhopadhyay, and A. Bayat, Characterization of an operational quantum resource in a critical many-body system, New J. Phys. **22**, 083077 (2020).
[42] R. Horodecki, P. Horodecki, M. Horodecki, and K. Horodecki, Quantum entanglement, Rev. Mod. Phys. **81**, 865 (2009).
[43] F. G. S. L. Brandão, M. Horodecki, J. Oppenheim, J. M. Renes, and R. W. Spekkens, The Resource Theory of Quantum States Out of Thermal Equilibrium, Phys. Rev. Lett. **111**, 250404 (2013).
[44] M. Horodecki and J. Oppenheim, (Quantumness in the context of) Resource theories, Int. J. Mod. Phys. B **27**, 1345019 (2013).
[45] E. Chitambar and G. Gour, Quantum resource theories, Rev. Mod. Phys. **91**, 025001 (2019).
[46] C. H. Bennett, H. J. Bernstein, S. Popescu, and B. Schumacher, Concentrating partial entanglement by local operations, Phys. Rev. A **53**, 2046 (1996).
[47] G. Vidal, Entanglement monotones, J. Mod. Opt. **47**, 355 (2000).
[48] O. Bohigas and M.-J. Giannoni, Chaotic motion and random matrix theories, in *Mathematical and Computational Methods in Nuclear Physics. Lecture Notes in Physics*, edited by J. S. Dehesa, J. M. G. Gomez, and A, Polls (Springer, Berlin, 1984), Vol. 209.
[49] T. Guhr, A. Muller-Groeling, and H. A. Weidenmuller, Random matrix theories in quantum physics: Common concepts, Phys. Rep. **299**, 189 (1998).
[50] M. V. Berry and M. Tabor, Level clustering in the regular spectrum, Proc. R. Soc. A **356**, 375 (1977).
[51] O. Bohigas, M. J. Giannoni, and C. Schmit, Characterization of Chaotic Quantum Spectra and Universality of Level Fluctuation Laws, Phys. Rev. Lett. **52**, 1 (1984).
[52] A. I. Larkin and Y. N. Ovchinnikov, Quasiclassical method in the theory of superconductivity, Sov. J. Exp. Theor. Phys. **28**, 1200 (1969).
[53] T. Nosaka, D. Rosa, and J. Yoon, The Thouless time for mass-deformed SYK, J. High Energy Phys. 09 (2018) 041.
[54] J. Kudler-Flam, L. Nie, and S. Ryu, Conformal field theory and the web of quantum chaos diagnostics, J. High Energy Phys. 01 (2020) 175.
[55] M. C. Bañuls, J. I. Cirac, and M. B. Hastings, Strong and Weak Thermalization of Infinite Nonintegrable Quantum Systems, Phys. Rev. Lett. **106**, 050405 (2011).
[56] D. N. Page, Average Entropy of a Subsystem, Phys. Rev. Lett. **71**, 1291 (1993).
[57] S. Sen, Average Entropy of a Subsystem, Phys. Rev. Lett. **77**, 1 (1996).
[58] K. Goto, A. Mollabashi, M. Nozaki, K. Tamaoka, and M. T. Tan, Information scrambling versus quantum revival through the lens of operator entanglement, J. High Energy Phys. 2022 (2022) 100.
[59] E. Mascot, M. Nozaki, and M. Tezuka, Local operator entanglement in spin chains, arXiv:2012.14609.